Ⅳ. 研究成果の刊行物・別刷

Vaccine 28 (2010) 2020–2025

Contents lists available at ScienceDirect

Vaccine

journal homepage: www.elsevier.com/locate/vaccine

Characterization of murine T-cell epitopes on mycobacterial DNA-binding protein 1 (MDP1) using DNA vaccination

Daisuke Suzuki[a,*], Toshi Nagata[b], Ghada Eweda[c], Sohkichi Matsumoto[d], Makoto Matsumoto[e], Kunio Tsujimura[c], Yukio Koide[c]

[a] 3rd Department of Internal Medicine, Hamamatsu University School of Medicine, 1-20-1 Higashi-ku, Handa-yama, Hamamatsu, Japan
[b] Department of Health Science, Hamamatsu University School of Medicine, 1-20-1 Higashi-ku, Handa-yama, Hamamatsu, Japan
[c] Department of Infectious Diseases, Hamamatsu University School of Medicine, 1-20-1 Higashi-ku, Handa-yama, Hamamatsu, Japan
[d] Department of Host Defense, Osaka City University Graduate School of Medicine, Osaka, Japan
[e] Otsuka Pharmaceutical Co., Ltd., Kagasuno 463-10 Kawauchi-cho, Tokushima, Japan

ARTICLE INFO

Keywords:
DNA immunization
T-cell epitope
Mycobacterium tuberculosis

ABSTRACT

Mycobacterial DNA-binding protein 1 (MDP1) is a major protein antigen in mycobacteria and induces protective immunity against *Mycobacterium tuberculosis* infection in mice. In this study we determined murine T-cell epitopes on MDP1 with MDP1 DNA immunization in mice. We analyzed interferon-γ production from the MDP1 DNA-immune splenocytes in response to 20-mer overlapping peptides covering MDP1 protein. We identified several CD4+ T-cell epitopes in three inbred mouse strains and one CD8+ T-cell epitope in C57BL/6 mice. These T-cell epitopes would be feasible for analysis of the role of MDP1-specific T-cells in protective immunity and for future vaccine design against *M. tuberculosis* infection.

1. Introduction

Tuberculosis (TB) has been one of the most serious infectious diseases in the world. There were estimated 9.2 million new causes and 1.7 million deaths from TB in 2006 [1]. One third of people in the world have been infected with *Mycobacterium tuberculosis* (Mtb), the causative agent of TB. Multidrug-resistant TB and co-infection of Mtb with human immunodeficiency virus are recent problems [1].

The only TB vaccine currently available is the attenuated *Mycobacterium bovis* strain Bacillus Calmette-Guérin (BCG). Although the BCG vaccine is the oldest and the most widely used vaccine [2], the effect of which has been questioned for preventing pulmonary TB in adults [3] and also to wane with time since vaccination [4]. Therefore, the improved vaccine is an urgent need against TB [5].

Cell-mediated immunity plays a pivotal role in the control of Mtb infection [6,7]. There is mounting evidence that CD4+ type 1 helper T (Th1) cells are involved in the development of resistance to the disease, primarily through the production of macrophage-activating cytokines such as interferon (IFN)-γ and tumor necrosis factor (TNF)-α. In addition, CD8+ cytotoxic T lymphocytes (CTL) contribute to disease resistance since susceptibility to Mtb is increased in mice with deficient in CD8+ T-cells [8].

Identification of protective antigens is a crucial step to develop effective vaccines against TB. Many protective antigen candidates have been reported. They include, secreted and membrane-bound proteins, virulence factors such as PE/PPE or EsX, or proteins expressed in host macrophages [9,10]. Since Mtb causes both acute disease and asymptomatic latent infection, antigens expressed in the dormant state have been also focused as target antigens for therapeutic vaccination of latent tuberculosis. Persisting bacilli resides within the hypoxic environment of the lung granulomas. Therefore, it is generally accepted that low-oxygen tension induces dormancy program of Mtb. Proteins expressed at the dormant stage include, two-component response regulator, dormancy survival regulator (*DosR*; Rv3133c) [11] and at least 20 other proteins encoded by the *DosR* regulon [12].

MDP1 is a major cellular protein of slow growers of mycobacteria [13]. The cellular content of MDP1 in mycobacterial cells increases at stationary and low-oxygen tension-induced non-replicating dormant phases [14]. MDP1 is a histone-like DNA-binding protein binding to GC-rich DNA and considered to control gene expression in mycobacteria [13,15]. MDP1 has an activity to suppress the growth rate of bacteria presumably by inhibiting macromolecular biosyntheses [16]. Recently, Lewin et al. [17] showed that reduction of MDP1 expression by antisense plasmid increased the growth of BCG in both broth culture and macrophages. They showed that the antisense DNA inhibited the

* Corresponding author. Tel.: +81 53 435 2335; fax: +81 53 435 2335.
E-mail address: zonxs@hama-med.ac.jp (D. Suzuki).

0264-410X/$ – see front matter © 2009 Elsevier Ltd. All rights reserved.
doi:10.1016/j.vaccine.2009.10.062

aggregation of BCG and reduced expression of several proteins in hypoxic condition as well, suggesting a role of MDP1 in regulation of gene expression in dormant bacilli. In addition to the role in the cytoplasm, MDP1 is exported by unknown mechanism to the cell wall and control the mycolic acid transfer [18] and mycobacterial adherence to lung epithelial cells [19]. Thus, MDP1 is a pleiotropic protein which has strong impacts on the mycobacterial virulence.

MDP1 has been also reported to be one of immunocompetent antigens. Prabhakar et al. [20] identified this protein as an immunodominant protein in human healthy contacts with TB patients through T-cell blot assay. They designated this protein as histone-like protein of Mtb (HLP_{Mt}), which is the same molecule as MDP1. Matsumoto et al. [21] found that CpG DNA enhances immunogenicity of MDP1, such as productivity of TNF-α and IL-6 from mouse macrophages. They showed that co-immunization of BALB/c and C3H/He mice with MDP1 and Mtb DNA elicited IFN-γ production specific for this protein and caused reduction of the bacterial burden following Mtb challenge [21].

DNA vaccination with gene gun bombardment is a reliable method to induce reproducible T-cell responses [22] and has been used for identification of T-cell epitopes of Mtb antigens, antigen (Ag) 85A [23–25], Ag85B [25], Ag85C [25], MPT51 [26,27], and *DosR* regulon-encoded proteins [28]. Here, we identified murine T-cell epitopes on MDP1 with a strategy using inbred mouse strains, gene gun immunization with expression plasmid DNA encoding MDP1, overlapping synthetic peptides spanning the entire mature MDP1 amino acid (aa) sequence, and major histocompatibility complex (MHC) binding peptide prediction algorithms.

2. Materials and methods

2.1. Animals

Inbred mouse strains, BALB/c, C57BL/6, and C3H/He, were purchased from Japan SLC (Hamamatsu, Japan). The mice were kept under specific pathogen-free conditions and fed autoclaved food and water *ad libitum* at the Institute for Experimental Animals of the Hamamatsu University School of Medicine. Two to three-month-old female mice were used in all experiments. Animal experiments were performed according to the Guidelines for Animal Experimentation, Hamamatsu University School of Medicine.

2.2. Plasmid

The DNA encoding MDP1 molecule was inserted between EcoRI and XhoI sites located downstream of cytomegalovirus immediate-early enhancer/promoter region of eukaryotic expression plasmid, pCI (Promega, Madison, WI, USA). The integrity of the nucleotide sequence was validated by automated DNA sequencing with ABI PRISM 310 genetic analyzer (Applied Biosystems, Foster City, CA, USA) using a dye primer cycle sequencing kit (Applied Biosystems).

2.3. Peptides

Peptides spanning the entire MDP1 aa sequence of BCG (205 aa residues) were synthesized as 20-mer peptides overlapping by 10 residues, with the exception of P6 (p46–65) and the carboxyl-terminal P21 (p186–205) ([15], Fig. 1). MDP1 p23–31 and p46–60 peptides were synthesized by Hayashi kasei (Osaka, Japan). All peptides were dissolved in phosphate-buffered saline (PBS) at a concentration of 10 mg ml^{-1} and stored at −80 °C until use.

2.4. Prediction of T-cell epitopes by MHC binding peptide prediction algorithms

For the prediction of murine T-cell epitopes, following MHC binding peptide prediction algorithms were used through their web sites. These are, National Institutes of Health BioInformatics and Molecular Analysis Section (BIMAS) ([29], http://bimas.dcrt.nig.gov/cgi-bin/molbio/ken_parker_comboform), SYFPEITHI program ([30], http://www.syfpeithi.de/), and RANKPEP program ([31], http://bio.dfci.harvard.edu/Tools/rankpep.html).

2.5. Immunization of mice

For DNA immunization with Helios gene gun system (Bio-Rad Laboratories, Hercules, CA, USA), preparation of the cartridge of DNA-coated gold particle cartridge was followed to the manufacturer's instruction manual. Finally, 0.5 mg of gold particles was coated with 1 μg of plasmid DNA and the injection was carried out with 0.5 mg gold per shot once. Mice were injected with 1 μg of plasmid DNA four times at 1-week intervals. Mice were also immunized subcutaneously with 10^6 CFU of BCG (Tokyo strain) twice at a 2-week interval.

2.6. Preparation of splenocyte culture supernatants

Spleen cells were harvested from mice. Recovered cells were cultured with RPMI medium supplemented with 10% fetal calf serum in 96-well plates at 2×10^6 cells/well in the presence or absence of 5 μg ml^{-1} of each MDP1 peptide at 37 °C with 5% CO_2 atmosphere. Supernatants were harvested 48 h later and stored at −20 °C until they were assayed. Concentration of IFN-γ in the culture supernatants was determined by a sandwich enzyme-linked immunosorbent assay (ELISA)

2.7. Quantification of IFN-γ with ELISA

The 96-well ELISA plates (EIA/RIA Plate A/2; Costar, Cambridge, MA) were coated with 2 μg ml^{-1} of capture antibody (Ab) (anti-murine IFN-γ monoclonal Ab [mAb] R4-6A2; BD Biosciences, San Jose, CA, USA) at 4 °C overnight, washed with PBS supplemented with 0.05% Tween 20 (PBS-Tween), and blocked with Block One Blocking solution (Nacalai Tesque, Kyoto, Japan) at room temperature for 45 min. After washed with PBS-Tween, the culture

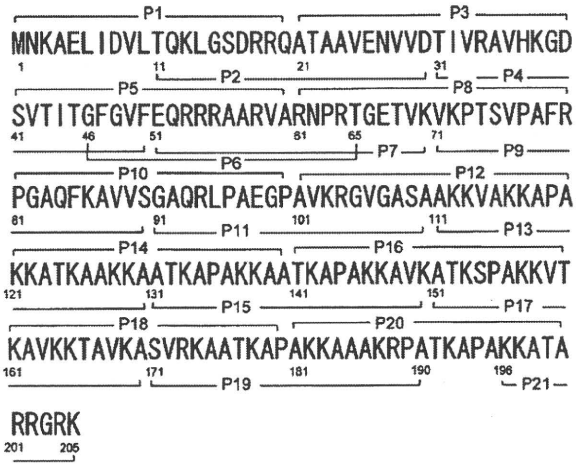

Fig. 1. Schematic representation of the 21 overlapping synthetic peptides from MDP1 of BCG. All peptides covering entire MDP1 of BCG (205 aa residues) were synthesized as 20-mer molecules overlapping by 10 amino acids with the neighboring peptides.

supernatants were added to the plates and the plates were incubated at 4 °C overnight. After washed with PBS-Tween, 0.5 μg ml^{-1} of biotin-labeled anti-murine IFN-γ mAb XMG1.2 (BD Biosciences) was added to the plates, and the plates were incubated for 1 h at room temperature. After washed with PBS-Tween, horseradish peroxidase-conjugated avidin (Bio-Rad Laboratories) was added and incubated for 30 min at room temperature. After washed, the plates were added with TMB one component HRP microwell substrate (BioFX Laboratories, Owings Mills, MD, USA) to detect bound horseradish peroxidase-conjugated streptavidin. After 5 min, the absorbance of each well was measured at 630 nm using an EZS-ABS Microplate Reader (Asahi Techno Glass Tokyo, Japan).

2.8. Depletion of CD4+ or CD8+ T-cell subsets

CD4+ or CD8+ T-cell subsets of peptide-reactive T-cells were determined by depletion of CD4+ or CD8+ T-cells, respectively. We used BD IMag system (BD Biosciences). Briefly, spleen cells were mixed thoroughly with anti-mouse CD4 particles-DM or anti-mouse CD8a particles-DM (BD Biosciences, 50 μl particles for 10^7 cells) and placed at 4 °C for 30 min. The labeled cells were placed on the BD IMagnet and incubated for 8 min. Supernatant was carefully removed. This supernatant contains the cell fraction which is devoid of CD4+ or CD8+ T-cells.

2.9. MHC stabilization assay

MHC stabilization assay is originally described in Ljunggren et al. [32]. RMA-S cells ([33], 10^6 cells/well) were cultured at 26 °C overnight and were then incubated for 1 h in the presence or absence of peptide (10, 50, or 100 μM). The cells were then transferred to 37 °C for 2 h and washed with FACS buffer, and cell surface expression of H2-D^b molecules was detected by flow cytometry by using phycoerythrin (PE)-conjugated mouse mAbs specific for H2-K^{d}D^b (28-14-8; eBioscience, San Diego, CA, USA). The results were expressed as the mean fluorescence intensity (MFI) ratio, which was determined as follows: MFI ratio = (MFI observed in the presence of peptide at 37 °C − MFI observed in the absence of peptide at 37 °C)/(MFI observed in the absence of peptide at 26 °C) × 100 (%).

2.10. Statistics

Data from multiple experiments were expressed as the means ± S.E.M. Data were analyzed with Student's unpaired *t*-test. *p* value of 0.05 or less was considered significant.

3. Results

3.1. IFN-γ production in response to overlapping synthetic peptides from MDP1 by splenocytes of pCI-MDP1 DNA-immune mice

Splenocytes from mice immunized with DNA vaccine encoding MDPI (pCI-MDP1) were stimulated with the overlapping MDP1 peptides for 48 h and IFN-γ concentration of culture supernatants was measured by ELISA. As shown in Fig. 2A, robust IFN-γ production was observed in splenocytes from MDP1 DNA-immune C57BL/6 mice (H2^b haplotype) in the presence of peptides P3 (p21–40), P9 (p71–90), and P11 (p91–110). Similarly, significantly higher IFN-γ production from splenocytes of MDP1 DNA-immune BALB/c (H2^d haplotype) and C3H/He (H2^k haplotype) mice were observed in response to two peptides, P5 (p41–60), P6 (p46–65) and three peptides, P5 (p41–60), P13 (p111–130), and P16 (p141–160), respectively (Fig. 2B and C). In C3H/He mice, P11 (p91–110) and P12 (p101–120) could induce relatively high IFN-γ production, but the value was not statistically significant.

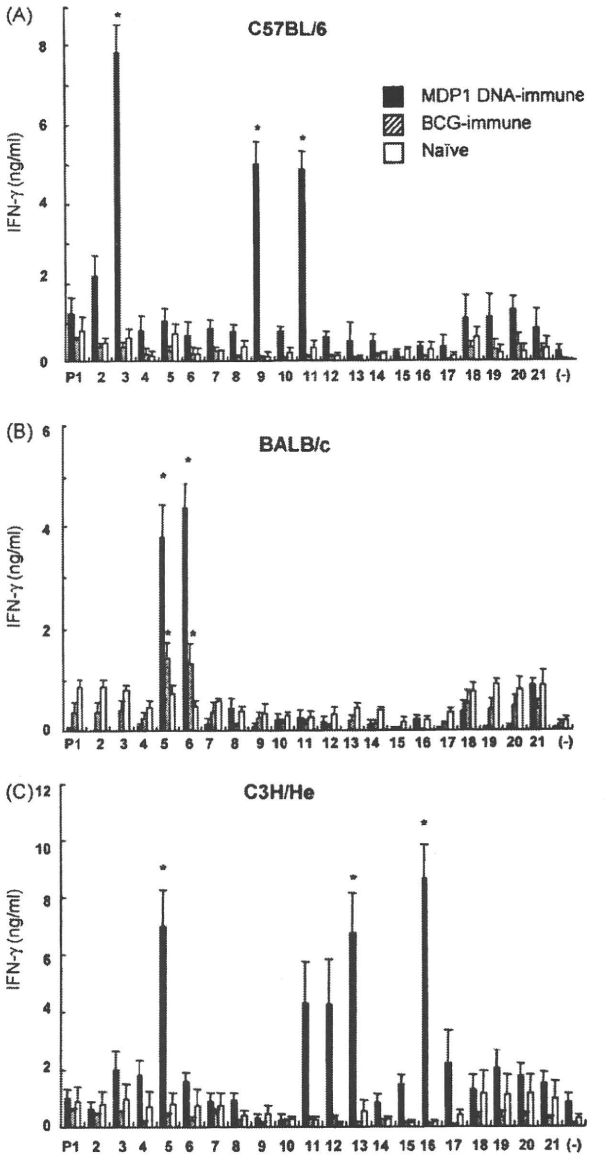

Fig. 2. IFN-γ production from splenocytes stimulated with overlapping peptides of MDP1. Inbred mice [C57BL/6 (A), BALB/c (B) and C3H/He (C)] were immunized with plasmid DNA encoding MDP1 using gene gun four times at 1-week intervals (filled bars) or with *M. bovis* BCG two times at a 2-week interval (hatched bars). The splenocytes (2×10^6) were stimulated with overlapping peptides (5 μg ml^{-1}) 2 weeks after the last immunization. Naïve mice (open bars) were used as controls. IFN-γ concentration of supernatant was analyzed by sandwich ELISA 48 h later. The means ± S.E.M. from three (C57BL/6, BALB/c) or six (C3H/He) mice are shown. Asterisks (*) indicate $p < 0.05$ compared with the value without peptide (-) with Student's unpaired *t*-test.

In order to examine whether the same peptide induce IFN-γ following natural mycobacterial infection, splenocytes from mice immunized with BCG were examined for IFN-γ production in response to MDP1 peptides. Two peptides, P5 and P6, also induced significant IFN-γ production from splenocytes of BCG-immune BALB/c mice (Fig. 2B), but the level of IFN-γ produced in BCG-immune mice was lower than that in MDP1 DNA-immune mice. We were not able to detect significant IFN-γ production from splenocytes of BCG-immune C57BL/6 and C3H/He mice (Fig. 2A and C). In this experimental condition, DNA immunization with MDP1 DNA was superior to BCG vaccination in terms of IFN-γ production level from splenocytes.

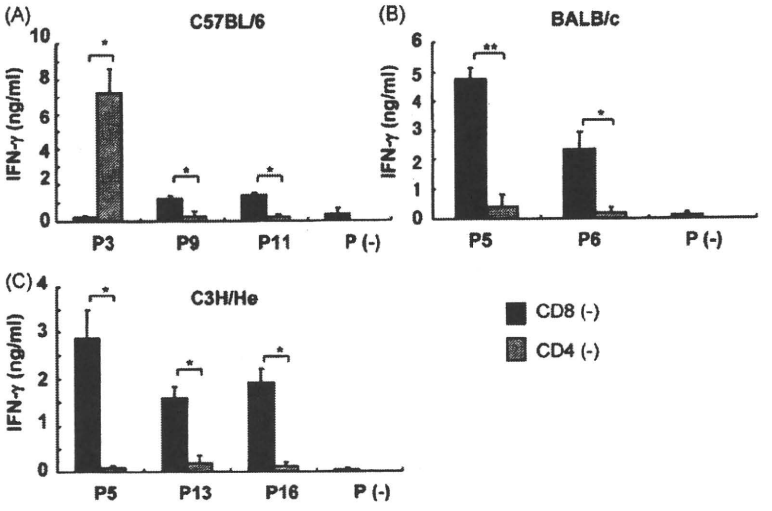

Fig. 3. Analysis of T-cell subsets responsive to MDP1 peptides. Mice were immunized with MDP1 DNA on the same schedule as Fig. 2. Splenocytes were treated with magnetic beads specific for CD4 or CD8. Cells (2×10^6) of the negative fraction were stimulated with peptides ($5\ \mu g\ ml^{-1}$). Amounts of IFN-γ in the supernatant were analyzed by sandwich ELISA 48 h later. The mean ± S.E.M. of three mice are shown. $^{**}p < 0.01$, $^{*}p < 0.05$ (Student's unpaired *t*-test).

3.2. T-cell subset analysis of T-cells by the depletion of CD4+ or CD8+ T-cells

Next, we examined which T-cell subsets responding to MDP1 peptides. CD4+ or CD8+ T-cells were removed with magnetic beads and residual cells were stimulated with MDP1 peptides and resultant IFN-γ production was compared. As shown in Fig. 3A, IFN-γ production from splenocytes of C57BL/6 mice in response to P3 (p21–40) was significantly decreased by depleting CD8+ T-cell subset. In contrast, IFN-γ production in response to P9 (p71–90) and P11 (p91–110) was decreased by depleting CD4+ T-cells. These results indicate that P3 contains CD8+ T-cell epitope, and P9 and P11 contain CD4+ T-cell epitopes. Intracellular IFN-γ staining results showed that IFN-γ-producing CD8+, but not CD4+ T-cells were observed in response to P3 in C57BL/6 mice. And IFN-γ-producing CD4+, but not CD8+ T-cells were observed in response to P9 and P11 (data not shown). Since C57BL/6 mice have a deletion of H2-Eα gene and do not express H2-E molecules on the cell surface [34], two CD4+ T-cell epitopes in these peptides are exclusively considered to be presented on H2-A^b.

In BALB/c mice, IFN-γ production in the presence of P5 (p41–60) and P6 (p46–65) was significantly reduced by depleting CD4+ T-cells. Similarly, IFN-γ production in the presence of P5 (p41–60), P13 (p111–130), or P16 (p141–160) was significantly reduced by depleting CD4+ T-cells in C3H/He mice (Fig. 3B and C). These results indicate that these peptide regions contain CD4+ T-cell epitopes.

3.3. Identification of minimal T-cell epitopes in the responsive peptide regions of MDP1

Generally, CD8+ T-cells recognize peptides of 8–11 aa residues on MHC class I molecules and CD4+ T-cells recognize peptides of 12–18 aa residues on MHC class II molecules. Several MHC binding peptide prediction algorithms are available on internet.

Table 1
T-cell epitope candidates in MDP1 molecule.

Peptide	Amino acid sequence	Estimated scores for restriction molecules[a]	
		K^b	D^b
p21–40 (P3)	ATAAVENVVDTIVRAVHKGD		
p23–31 (9-mer)	AAVENVVDT	**0.13**	**108** 20
p23–32 (10-mer)	AAVENVVDTI	**0.40**	**50.2** 33
		A^d	E^d
p41–60 (P5)	SVTITGFGVFEQRRRAARVA		
p46–65 (P6)	GFGVFEQRRRAARVARNPRT		
p52–60	QRRRAARVA	11.9 (7.1)	–[b]
		A^k	E^k
p41–60 (P5)	SVTITGFGVFEQRRRAARVA		
p44–58 (15-mer)	ITGFGVFEQRRRAAR		24
GFGVFEQRR	10.8 (14.2)		
p111–130 (P13)	KKVAKKAPAKKATKAAKKAA	A^k	E^k
p113–121 (9-mer)	VAKKAPAKK	–	17.9 (10)
p116–124 (9-mer)	KAPAKKATK	–	25.4 (10)
p121–129 (9-mer)	KKATKAAKK	–	18.7 (10)
p141–160 (P16)	TKAPAKKAVKATKSPAKKVT	A^k	E^k
p142–150 (9-mer)	KAPAKKAVK	–	17.3 (10)
p145–153 (9-mer)	AKKAVKATK	–	15.9 (10)

Epitopes predicted by computer algorithms are shown.
[a] Estimated scores are derived from BIMAS (bold), SYFPEITHI (underlined), or RANKPEP (plain). Parentheses indicate threshold scores, scores above which suggest the peptide binding to the corresponding H2 molecule.
[b] Score not shown in the program.

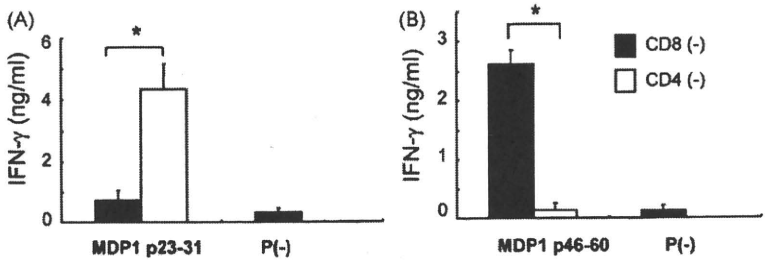

Fig. 4. IFN-γ production from T-cells in the presence of predicted peptides, MDP1 p23–31 and p46–60 peptides. C57BL/6 and BALB/c mice were immunized with MDP1 DNA and the immune splenocytes were treated with magnetic beads specific for CD4 or CD8α and purified the negative fraction. Cells (2×10^6) of the fraction were stimulated with 5 μg ml^{-1} of MDP1 p23–31 and MDP1 p46–65. IFN-γ in the culture supernatant was analyzed by sandwich ELISA 48 h later. The mean ± S.E.M. of three mice are shown. Asterisks (*) indicate $p < 0.05$ compared with the value without peptide (-) with Student's unpaired *t*-test.

We employed BIMAS and SYFPEITHI programs for prediction of CD8+ T-cell epitope(s) in P3 in C57BL/6 mice and RANKPEP program for CD4+ T-cell epitope(s) in P5 and P6 regions in BALB/c mice (Table 1). MDP1 p23–31 9-mer peptide (AAVENVVDT) in P3 region showed the highest score (108) for H2-D^b binding in BIMAS program (Table 1). In BALB/c mice, RANKPEP algorithm predicted MDP1 p52–60 as the core motif of H2-A^d-restricted CD4+ T-cell epitope (Table 1). Since both P5 (p41–60) and P6 (p46–65) peptides let the immune splenocytes produce IFN-γ, we prepared overlapping 15-mer peptide (p46–60) and examined the capacity to induce IFN-γ production from immune splenocytes.

As shown in Fig. 4A, CD8+ T-cells of MDP1 DNA-immune C57BL/6 mice produced significant amounts of IFN-γ in response to MDP1 p23–31 peptide. Splenocytes of the immune mice in the absence of the peptide and splenocytes of naïve C57BL/6 mice with or without the peptide did not produce significant level of IFN-γ (data not shown). Similarly, CD4+ T-cells of MDP1 DNA-immune BALB/c mice produced significant amounts of IFN-γ in response to MDP1 p46–60 peptide (Fig. 4B). Splenocytes of the immune mice in the absence of the peptide and splenocytes of naïve BALB/c mice with or without the peptide did not produce significant level of IFN-γ (data not shown). These results indicate that MDP1 p23–31 is a minimal *bona fide* CD8+ T-cell epitope in C57BL/6 mice and MDP1 p46–60 is CD4+ T-cell epitope in BALB/c mice, respectively.

As for C3H/He mice, RANKPEP program predicted that MDP1 p41–60 contains MDP1 p46–54 peptide which showed the highest score (10.8) in MDP1 peptides presented on H2-A^k. However, the score was less than the peptide binding threshold value (14.2), suggesting no binding. The SYFPEITHI program, which has the prediction program for H2-A^k and E^k, predicted MDP1 p44–58 15-mer peptide as H2-E^k binder with the highest score (24) in the program (Table 1). RANKPEP program also predicted three core 9-mer peptides restricted by H2-E^k, MDP1 p113–121, p116–124, and p121–129 in P13 (p111–130) region and two core peptides restricted by H2-E^k, MDP1 p142–150 and p145–153 in P16 (p141–160) region, respectively (Table 1).

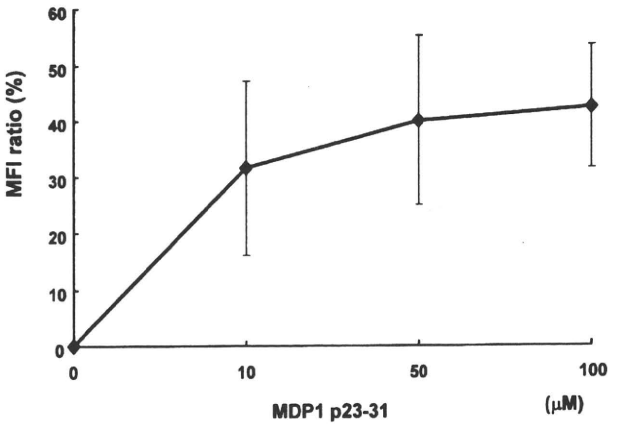

Fig. 5. MHC binding assay of MDP1 p23–31 to H2-D^b. The ability of MDP1 p23–31 for binding to H2-D^b was measured by determining the stabilization of class I molecules on the surfaces of TAP2-deficient RMA-S. RMA-S cells (10^6 cells/well) were cultured at 26 °C overnight and then were incubated for 1 h in the presence or absence of peptide (10, 50 or 100 μM). The cells were then transferred to 37 °C for 2 h and washed with FACS buffer, and cell surface expression of H2-D^b was detected by flow cytometry by using a phycoerythrin-conjugated mAb specific for H2-K^{d}D^b. The results were expressed as MFI ratio ± SD.

3.4. *Identification of an MHC class Ia restriction molecule for MDP1 p23–31 in C57BL/6 mice*

Since MDP1 p23–31 was found to be a CD8+ T-cell epitope for C57BL/6 mice, we examined MHC binding assay to determine H2 restriction molecule for the peptide. As shown in Fig. 5, the MFI ratio of PE-conjugated anti-H2-D^b mAb increased in the presence of 10 μM of MDP1 p23–31 peptide. This value further increased up to 42.5% in the presence of 100 μM of the peptide. This result confirmed that MDP1 p23–31 peptide does bind to H2-D^b.

4. Discussion

T-cells play pivotal role in induction of protective immunity against intracellular pathogens such as Mtb [6,7]. The protective immunity induced by MDP1 immunization would be mainly attributable to T-cell responses evoked by the immunization. We here determined murine T-cell epitopes of MDP1, which would give the concrete basis of the protective immunity by MDP1 immunization. The peculiar immunogenic feature of MDP1 is DNA-dependent augmentation of antigenicity. MDP1 elicited protective immune responses when it was vaccinated to BALB/c and C3H/He mice with genomic DNA derived from *M. tuberculosis* [21]. Up-regulation of antigen-presenting cell functions induced by the interaction between MDP1 and CpG DNA was suggested in the protective immune responses [21]. CpG DNA is a key component of DNA vaccines for evoking significant immune responses against antigens. Therefore, we considered that DNA vaccination of MDP1 induce substantial immune responses, because produced MDP1 proteins may bind to CpG DNA in plasmid backbone and enhance the adjuvant effects.

In this study, we found at least seven T-cell epitope candidates peptides upon MDP1 DNA immunization. By contrast, only one peptide region (MDP1 p41–65) was found with *M. bovis* BCG vaccination (Fig. 2B). Several reasons for this difference would be speculated. First, MDP1 localizes in the cytoplasmic space, or is tightly attached to the cell wall of the live *Mycobacterium*. Non-secreted antigens like MDP1 would be difficult to be immunoreactive in the form of BCG vaccine. Second, BCG vaccine has been reported to be

inefficient in terms of MHC class I antigen presentation. The fact may also cause the difference in the T-cell responses. Other possible explanation is that living mycobacteria have the mechanism to hide immunogenicity of MDP1, because strong immune response to MDP1 causes bactericidal host response.

In C57BL/6 mice, we found one CD8+ T-cell epitope, MDP1 p23–31 and two CD4+ T-cell epitopes, MDP1 p71–90 and MDP1 p91–110. MDP1 p23–31 (AAVENVVDT) was speculated to be presented on H2-D^b with prediction algorithms and this was confirmed with MHC binding assay. Reported dominant peptide binding motif of H2-D^b consists of asparagine at position 5 (P5) and hydrophobic C-terminal residue such as isoleucine or leucine (P9 or P10) [35,36]. P5 of MDP1 p23–31 is asparagine, but the C-terminal residue does not fit the motif. P5 (asparagine) and P10 (isoleucine) of MDP1 p23–32 fit the motif, suggesting that MDP1 p23–32 peptide also works as CD8+ T-cell epitope.

In BALB/c mice, MDP1 p46–60 was identified as H2-A^d-restricted CD4+ T-cell epitope. Since both P5 (p41–60) and P6 (p46–65) peptides, but not P7 (p51–70) peptide, let the immune splenocytes produce IFN-γ, we reasoned that the N-terminal aa residues (p46–50) are critical for the function. In C3H/He mice, at least three CD4+ T-cell epitopes were identified. RANKPEP or SYFPEITHI programs predicted P5 (p41–60), P13 (p111–130), and P16 (p141–160) bind to H2-E^k.

In conclusion, we identified murine T-cell epitopes of MDP1, an immunogenic major cellular mycobacterial protein causing protective immunity. We identified several CD4+ T-cell epitopes in three inbred mouse strains and one CD8+ T-cell epitope in C57BL/6 mice. Previously, we reported murine T-cell epitopes of MPT51, which is one of major secreted mycobacterial proteins at acute phase TB. MDP1 is a very abundant cellular protein and has been reported to be even up-regulated in dormant stage mycobacteria. Therefore, T-cell epitopes of MPT51 and MDP1 would be feasible for analysis of T-cell responses in different stage Mtb and for future TB vaccine design.

Acknowledgements

This work was supported by grants-in-aid for scientific research from the Japanese Society for the Promotion of Science (grant 20590438 to T. N. and grant 20390125 to Y. K.), a grant-in-aid for the Centers of Excellence (COE) Research Program from the Ministry of Education, Culture, Sports, Science and Technology of Japan, and a grant-in-aid from the United States-Japan Cooperative Medical Science Program.

References

[1] World Health Organization. WHO Report 2007 Global tuberculosis control: surveillance, planning, financing. Geneva; 2008 [online]. http://www.who.intentity/tb/publications/global_report/2008/pdf/fullreport.pdf (accessed 15.11.2008).
[2] Bloom BR, Fine PEM. The BCG experience: implications for future vaccines against tuberculosis. In: Tuberculosis: pathogenesis, protection, and control. Washington, DC: ASM Press; 1994. p. 531–57.
[3] Andersen P, Doherty TM. The success and failure of BCG—implications for a novel tuberculosis vaccine. Nat Rev Microbiol 2005;3:656–62.
[4] Sterne JAC, Rodrigues LC, Guedes IN. Does the efficacy of BCG decline with time since vaccination? Int J Tuberc Lung Dis 1998;2:200–7.
[5] Andersen P. Tuberculosis vaccines—an update. Nat Rev Microbiol 2007;5:484–7.
[6] Kaufmann SHE. How can immunology contribute to the control of tuberculosis? Nat Rev Immunol 2001;1:20–30.
[7] Kaufmann SHE. Immunity to intracellular bacteria. In: Paul WE, editor. Fundamental immunology. 5th ed. Philadelphia: Lippincott Williams & Wilkins Publishers; 2003. p. 1229–61.
[8] Kaufumann SHE, Flynn JL. CD8 T cells in tuberculosis. In: Cole ST, Eisenach KD, McMurray DN, Jacobs Jr WR, editors. Tuberculosis and the tubercle bacillus. Washington, DC: ASM Press; 2005. p. 465–74.
[9] Andersen P, Doherty TM. TB subunit vaccines—putting the pieces together. Microbes Infect 2005;7:911–21.
[10] Sable SB, Karlra M, Verma I, Khuller GK. Tuberculosis subunit vaccine design: the conflict of antigenicity and immunogenicity. Clin Immunol 2007;122:239–51.
[11] Park HD, Guinn KM, Harrell MI, Liao R, Voskuil MI, Tompa M, et al. Rv3133c/*dosR* is a transcription factor that mediates the hypoxic response of *Mycobacterium tuberculosis*. Mol Microbiol 2003;48:833–43.
[12] Karakousis PC, Yoshimatsu T, Lamichhane G, Woolwine SC, Nuermberger EL, Grosset J, et al. Dormancy phenotype displayed by extracellular *Mycobacterium tuberculosis* within artificial granulomas in mice. J Exp Med 2004;200:647–57.
[13] Matsumoto S, Yukitake H, Furugen M, Matsuo T, Mineta T, Yamada T. Identification of a novel DNA-binding protein from *Mycobacterium bovis* Bacillus Calmette-Guérin. Mirobiol Immunol 1999;43:1027–36.
[14] Lee BH, Murugasu-Oei B, Dick T. Upregulation of a histone-like protein in dormant *Mycobacterium smegmatis*. Mol Gen Genet 1998;260:475–9.
[15] Furugen M, Matsumoto S, Matsuo T, Matsumoto M, Yamada T. Identification of the mycobacterial DNA-binding protein 1 region which suppresses transcription in vitro. Microb Path 2001;30:129–38.
[16] Matsumoto S, Furugen M, Yukitake H, Yamada T. The gene encoding mycobacterial DNA-binding protein I (MDP I) transformed rapidly growing bacteria to slowly growing bacteria. FEMS Microbiol Lett 2000;182:297–301.
[17] Lewin A, Baus D, Kamal E, Bon F, Kunisch R, Maurischat S, et al. The mycobacterial DNA-binding protein I (MDPI) from *Mycobacterium bovis* BCG influences various growth characteristics. BMC Microbiol 2008;8:91–102.
[18] Katsube T, Matsumoto S, Takatsuka M, Okuyama M, Ozeki Y, Naito M, et al. Control of cell wall assembly by a histone-like protein in Mycobacteria. J Bacteriol 2007;189:8241–9.
[19] Aoki K, Matsumoto S, Hirayama Y, Wada T, Ozeki Y, Niki M, et al. Extracellular mycobacterial DNA-binding protein 1 participates in *Mycobacterium*-lung epithelial cell interaction through hyaluronic acid. J Biol Chem 2004;279:39798–806.
[20] Prabhakar S, Annapurna PS, Jain NK, Dey AB, Tyagi JS, Prasad HK. Identification of an immunogenic histone-like protein (HLP_{Mt}) of *Mycobacterium tuberculosis*. Tuberc Lung Dis 1998;79:43–53.
[21] Matsumoto S, Matsumoto M, Umemori K, Ozeki Y, Furugen M, Tatsuo T, et al. DNA augments antigenicity of mycobacterial DNA-binding protein 1 confers protection against *Mycobacterium tuberculosis* infection in mice. J Immunol 2005;175:441–9.
[22] Yoshida A, Nagata T, Uchijima M, Higashi T, Koide Y. Advantage of gene gun-mediated over intramuscular inoculation of plasmid DNA vaccine in reproducible induction of specific immune responses. Vaccine 2000;18:1725–9.
[23] Denis O, Tanghe A, Palfliet K, Jurion F, van den Berg TP, Vanonckelen A, et al. Vaccination with plasmid DNA encoding mycobacterial antigen 85A stimulates a $CD4^+$ and $CD8^+$ T-cell epitopic repertoire broader than that stimulated by *Mycobacterium tuberculosis* H37Rv infection. Infect Immun 1998;66:1527–33.
[24] Tanghe A, D'Souza S, Rosseels V, Denis O, Ottenhoff TH, Dalemans W, et al. Improved immunogenicity and protective efficacy of a tuberculosis DNA vaccine encoding Ag85 by protein boosting. Infect Immun 2001;69:3041–7.
[25] D'Souza S, Rosseels V, Romano M, Tanghe A, Denis O, Jurion F, et al. Mapping of murine Th1 helper T-cell epitopes of mycolyl transferases Ag85A, Ag85B, and Ag85C from *Mycobacterium tuberculosis*. Infect Immun 2003;71:483–93.
[26] Suzuki M, Aoshi T, Nagata T, Koide Y. Identification of murine H2-D^d- and H2-A^b-restricted T-cell epitopes on a novel protective antigen, MPT51, of *Mycobacterium tuberculosis*. Infect Immun 2004;72:3829–37.
[27] Aoshi T, Nagata T, Suzuki M, Uchijima M, Hashimoto D, Rafiei A, et al. Identification of an HLA-A*0201-restricted T-cell epitope on MPT51 protein, a major secreted protein derived from *Mycobacterium tuberculosis* by MPT51 overlapping peptide screening. Infect Immun 2008;76:1565–71.
[28] Roupie V, Romano M, Zhang L, Korf H, Lin MY, Franken KL, et al. Immunogenicity of eight dormancy regulon-encoded proteins of *Mycobacterium tuberculosis* in DNA-vaccinated and tuberculosis-infected mice. Infect Immun 2007;75:941–9.
[29] Parker KC, Bednarek MA, Coligan JE. Scheme for ranking potential HLA-A2 binding peptides based on independent binding of individual peptide side-chains. J Immunol 1994;152:163–75.
[30] Rammensee H-G, Bachmann J, Emmerich NPN, Bachor OA, Sevanović S. SYFPEITHI: database for MHC ligands and peptide motifs. Immunogenetics 1999;50:213–9.
[31] Reche PA, Glutting J-P, Zhang H, Reinherz EL. Enhancement to the RANKPEP resource for the prediction of peptide binding to MHC molecules using profiles. Immunogenetics 2004;56:405–19.
[32] Ljunggren HG, Stam NJ, Ohlen C, Neefjes JJ, Hglund P, Heemels MT, et al. Empty MHC class I molecules come out in the cold. Nature 1990;346:476–80.
[33] Ljunggren H-G, Kärre K. Host resistance directed selectively against H-2-deficient lymphoma variants. J Exp Med 1985;162:1745–59.
[34] Mathis DJ, Benoist C, Williams II VE, Kanter M, McDevitt HO. Several mechanisms can account for defective *Eα* gene expression in different mouse haplotypes. Proc Natl Acad Sci USA 1983;80:273–7.
[35] Rammensee H-G, Friede T, Stevanović S. MHC ligands and peptide motifs: first listing. Immunogenetics 1995;41:178–228.
[36] Margulies DH, McClusky J. The major histocompatibility complex and its encoded proteins. In: Paul WE, editor. Fundamental Immunology. 5th ed. Philadelphia: Lippincott Williams & Wilkins Publishers; 2003. p. 571–612.

Microbiology and Immunology

Microbiol Immunol 2010; **54**: 170–174
doi:10.1111/j.1348-0421.2009.00199.x

NOTE

Differential recruitment of CD63 and Rab7-interacting-lysosomal-protein to phagosomes containing *Mycobacterium tuberculosis* in macrophages

Shintaro Seto[1], Sohkichi Matsumoto[2], Kunio Tsujimura[1] and Yukio Koide[1]

[1]Department of Infectious Diseases, Hamamatsu University School of Medicine, 1-20-1 Handayama, Higashi-ku, Hamamatsu, 431-3192, and [2]Department of Bacteriology, Osaka City University Graduate School of Medicine, 1-4-3, Asahi-machi, Abeno-ku, Osaka 545-8585, Japan

ABSTRACT

***M.tb* is an intracellular pathogen which survives within the phagosomes of host macrophages by inhibiting their fusion with lysosomes. Here, it has been demonstrated that a lysosomal glycoprotein, CD63, is recruited to the majority of *M.tb* phagosomes, while RILP shows limited localization. This is consistent with the author's findings that CD63, but not RILP, is recruited to the phagosomes in macrophages expressing the dominant negative form of Rab7. These results suggest that *M.tb* phagosomes selectively fuse with endosomes and lysosomes to escape killing activity while acquiring nutrients.**

Key words lysosome, macrophage, *Mycobacterium tuberculosis*, phagosome.

Phagocytosis of infected pathogens by macrophages plays an important role in the early stages of innate immunity. Phagocytosed pathogens are incorporated into phagosomal vacuoles. These phagosomes then interact with endosomal and lysosomal vesicles in a process referred to as phagolysosome biogenesis. During phagolysosome biogenesis, phagosomes acquire degradative and microbicidal properties, leading phagocytosed pathogens to be killed and degraded.

M.tb, the causative bacterium of tuberculosis, infects more than one-third of the human population. *M.tb* is able to survive and proliferate within phagosomes of the host's macrophages by inhibiting phagolysosome biogenesis (1, 2). However, the exact process by which *M.tb* blocks phagolysosome biogenesis is not fully understood. Recently, it was reported that phagosomes containing *M.tb* (*M.tb* phagosomes) within dendritic cells are associated with lysosomes in the early stages of infection (3). In addition, we have previously demonstrated that LAMP-2, but not cathepsin D, is recruited to *M.tb* phagosomes in macrophages (4). These results suggest that *M.tb* phagosomes selectively fuse with lysosomal vesicles which have distinct characteristics. To investigate this possibility, we further examined the localization of two lysosomal marker proteins, CD63 and RILP, on *M.tb* phagosomes in this study.

Raw264.7 macrophage was obtained from the American Type Culture Collection (Manassas, VA, USA) and maintained in Dulbecco's modified Eagle's medium supplemented with 10% FBS (Invitrogen, Carlsbad, CA, USA), 25 μg/ml penicillin G, and 25 μg/ml streptomycin at 37°C in 5% CO_2. *M.tb* strain H37Rv and *Mycobacterium smegmatis* mc^2155 were grown in 7H9 medium supplemented with 10% Middlebrook ADC (BD Biosciences, San Jose, CA, USA), 0.5% glycerol, 0.05% Tween 80 (mycobacteria complete medium) at 37°C. *M tb* strain H37Rv transformed with a plasmid encoding DsRed (5) was grown in mycobacteria complete medium with 25 μg/ml kanamycin at 37°C. To construct the plasmids encoding CD63-EGFP and EGFP-RILP, PCR

Correspondence
Yukio Koide, Executive Director, Hamamatsu University School of Medicine, 1-20-1 Handayama, Higashi-ku, Hamamatsu, 431-3192, Japan.
Tel: +81 53 435 2101; fax: +81 53 435 2101; email: koidelb@hama-med.ac.jp

Received 27 October 2009; revised 18 November 2009; accepted 20 November 2009.

List of Abbreviations: CLSM, confocal laser scanning microscopy; LAMP-2, lysosomal associated membrane protein-2; *M. smegmatis*, *Mycobacterium smegmatis*; *M.tb*, *Mycobacterium tuberculosis*; MTOC, microtubule-organizing center; RILP, Rab7-interacting-lysosomal-proteins.

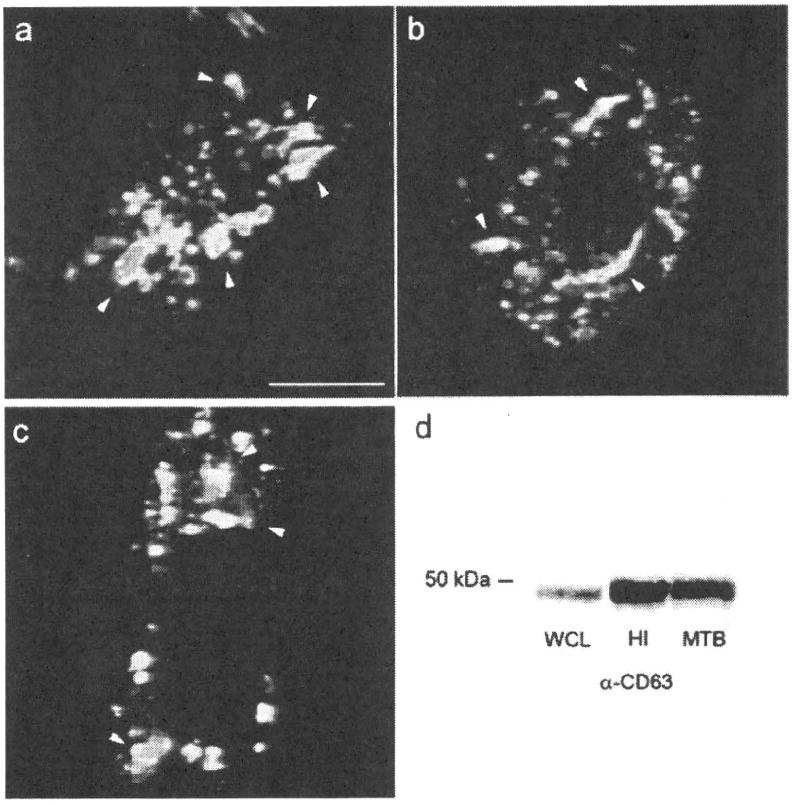

Fig. 1. Localization of CD63 on *M.tb* phagosomes. (a, b) Raw264.7 macrophages expressing CD63-EGFP were infected with *M.tb* expressing DsRed for (a) 30 min and (b) 6 hr. Infected cells were fixed and observed by CLSM. (c) *M.tb*-infected Raw264.7 macrophages were stained with anti-CD63 and Alexa488-conjugated anti-rat IgG antibodies and observed by CLSM. Arrowheads indicate CD63-positive phagosomes; scale bar, 10 μm. (d) CD63 localization in isolated mycobacterial phagosome fractions. Whole cell lysates from Raw264.7, the heat-inactivated *M. smegmatis* phagosome and live *M.tb* phagosome fractions were subjected to SDS-PAGE, followed by immunoblotting using anti-CD63 antibody. HI, heat-inactivated *M. smegmatis* phagosome fraction; MTB, live *M.tb* phagosome fraction; WCL, Raw264.7.

was carried out using cDNA derived from HeLa cells as a template and the following primer sets: human CD63 (5′-CCTCGAGCCACCATGGCGGTGGAAGGAGGAATGAAATG-3′ and 5′-CGGATCCCCATCACCTCGTAGCCACTTCTGATAC-3′), and human RILP (5′-CAGATCTATGGAGCCCAGGAGGGCGGC-3′ and 5′-CGAATTCTCAGGCCTCTGGGGCGGCTG-3′). The PCR products of CD63 and RILP were inserted into pEGFP-N2 and pEGFP-C1 vectors (Clontech, Mountain View, CA, USA), respectively. Transfection of macrophages with plasmids, infection of bacteria with transfected macrophages, CLSM, immunofluorescence microscopy, and isolation of mycobacterial phagosomes were performed as described previously (4). For immunofluorescence microscopy, macrophages were stained with rat anti-CD63 monoclonal antibody (1:30 v/v, MBL, Nagoya, Japan) and Alexa488-conjugated anti-rat IgG antibody (1:1000 v/v, Invitrogen). For immunoblotting analysis, aliquots of 40 μg of cell lysates from Raw264.7 and 15 μg of phagosomal fraction proteins were separated by SDS-PAGE and then subjected to immunoblotting analysis using rat anti-CD63 monoclonal antibody (1:100 v/v, MBL). The unpaired two-sided Student's *t*-test was used to assess the statistical significance of the differences between the two groups.

CD63 has been shown to be localized to the phagosome during phagolysosome biogenesis (2, 6), but its localization on live mycobacterial phagosomes is still controversial (2, 3, 7). CD63 was originally identified as a platelet activation marker (8) and has also been used as a marker for late endosomes and lysosomes because of its function in phagosome acidification (9–12). We therefore re-assessed CD63 localization on *M.tb* phagosomes in infected macrophages (Fig. 1). Raw264.7 macrophages transfected with a plasmid encoding CD63-EGFP were infected with *M.tb* expressing DsRed. Infected cells were fixed and observed by CLSM. Clear CD63 localization was observed on more than 60% of *M.tb* phagosomes at 30 min and 6 hr post infection (Fig. 1a, b). To rule out the possibility that CD63 localization on *M.tb* phagosomes is caused by exogenous expression of CD63-EGFP, immunofluorescence microscopy with anti-CD63 antibody was performed (Fig. 1c). We found that endogenous CD63 was also localized to about 60% of *M.tb* phagosomes at 6 hr post infection. To confirm the recruitment of CD63 to live *M.tb* phagosomes biochemically, we carried out

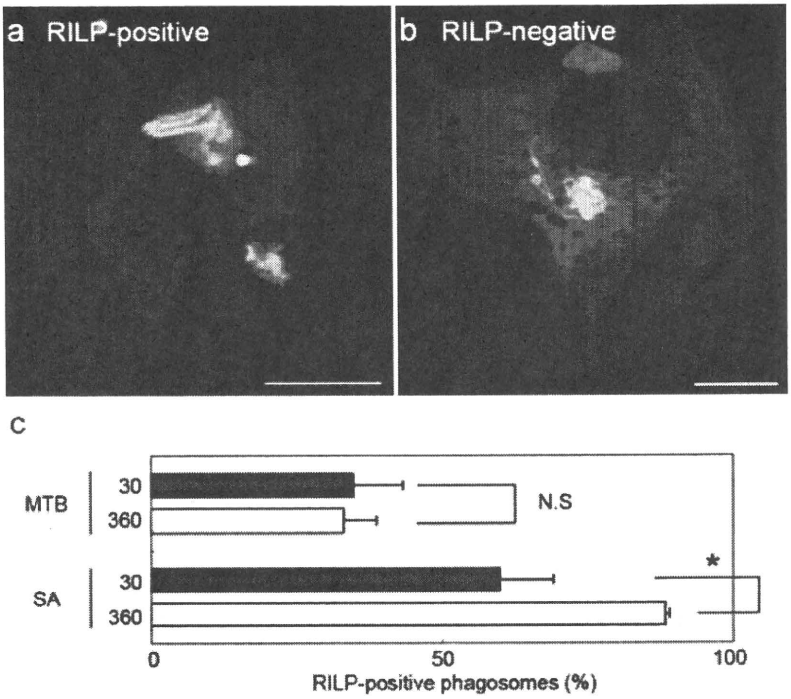

Fig. 2. Localization of RILP on *M.tb* phagosomes. (a, b) Raw264.7 macrophages expressing EGFP-RILP were infected with *M.tb* expressing DsRed. Infected cells were fixed and observed by CLSM. (a) and (b) show representative cell images of RILP-positive and RILP-negative *M.tb* phagosomes, respectively. Scale bar, 10 μm. (c) The proportion of RILP-positive phagosomes of *M.tb* and *Staphylococcus aureus* at 30 min and 360 min postinfection. *, $P < 0.05$; MTB, proportion of RILP-positive phagosomes of *M.tb;* N.S, no significant difference between the groups; SA, proportion of RILP-positive phagosomes of *Staphylococcus aureus*.

immunoblotting analysis for CD63 in isolated mycobacterial phagosome fractions (Fig. 1d). Raw264.7 macrophages were allowed to phagocytose heat-inactivated *M. smegmatis* or infected with *M.tb* for 6 hr, and the phagosomal fractions isolated as described previously (4, 13). Proteins extracted from isolated phagosomal fractions were subjected to immunoblotting analysis using anti-CD63 antibody. Immunoblotting analysis revealed that CD63 is recruited to live *M.tb* phagosomes as well as to heat-inactivated *M. smegmatis* phagosomes. These results suggest that *M.tb* phagosomes fuse with CD63-positive lysosomal vesicles.

RILP interacts with the active form of Rab7 and mediates the fusion of endosomes with lysosomes (14, 15). RILP is also reported to be localized to the phagosome and to recruit the minus-end motor complex dynein-dynactin to the phagosome, resulting in migration of the phagosome to the MTOC where late endosomal and lysosomal vesicles accumulate (16). In the process of recruitment of RILP to the phagosome, tubular vesicles expressing RILP have been observed to be elongated from the MTOC, fusing with the phagosome (16). RILP has been reported to be absent from the *Mycobacterium bovis* strain BCG phagosome despite Rab7 localization (17). We have previously shown that Rab7 is transiently recruited to, and subsequently released from, *M.tb* phagosomes (4), but the interaction of RILP with *M.tb* phagosomes has not been previously reported. We examined the subcellular localization of EGFP-RILP in macrophages infected with *M.tb* (Fig. 2). In *M.tb*-infected macrophages, RILP-positive phagosomes appeared and increased to 30% of *M.tb* phagosomes up until 30 min post infection (Fig. 2a, c). No further increase was seen after this time (Fig. 2b, c). On the other hand, the proportion of RILP-positive *Staphylococcus aureus* phagosomes continued to increase beyond 30 min post infection (Fig. 2c). We also found that the proportion of RILP-positive phagosomes containing heat-inactivated *M.tb* reached more than 80% at 6 hr post infection. These results suggest that further recruitment of RILP to phagosomes containing live *M.tb* after 30 min post infection might be actively inhibited.

Next, we examined whether recruitment of CD63 and RILP to phagosomes depends on the function of Rab7 in macrophages. Raw264.7 macrophages transfected with two plasmids encoding either EGFP-fused CD63 or RILP and a dominant-negative form of Rab7, Rab7T22N, were allowed to phagocytose latex-beads for 2 hr and were then examined by CLSM for localization of lysosomal proteins on the phagosomes. Both lysosomal markers were localized to latex-bead-containing phagosomes in the control cells (Fig. 3a-1, b-1). CD63 was found on the majority of latex-bead-containing phagosomes in the cells expressing Rab7T22N (Fig. 3a-2, a-3), as well as in the control cells. However, consistent with previous findings, RILP

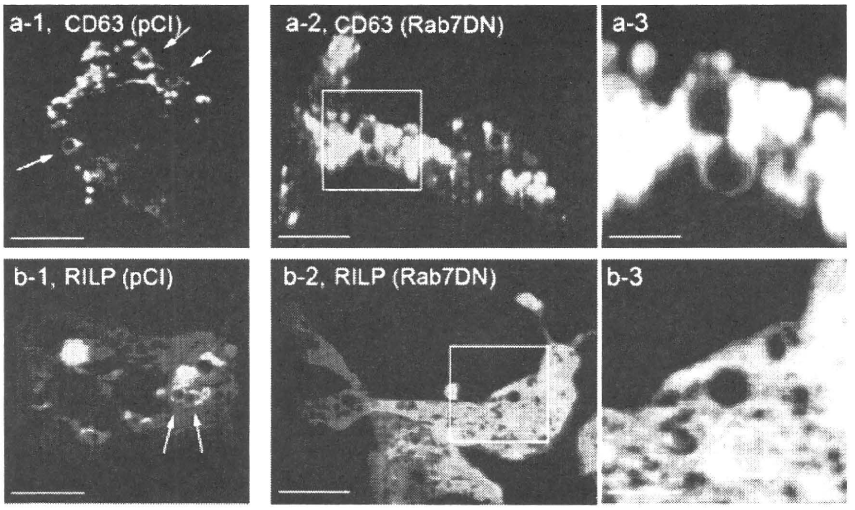

Fig. 3. Localization of lysosomal markers on latex-bead-containing phagosomes in Raw264.7 macrophages expressing dominant-negative Rab7. Raw264.7 macrophages expressing (a-2, a-3) Rab7T22N together with CD63-EGFP or (b-2, b-3) EGFP-RILP were allowed to phagocytose latex beads. Cells were fixed 2 hr after phagocytosis and observed by CLSM. (a-1, b-1) Cell images transfected with a control plasmid instead of the plasmid expressing Rab7T22N. (b-3, c-3) Enlarged images of phagosomes presented in b-2 and c-2, respectively. Scale bar, 10 μm (left and middle), 3 μm (right). pCI, cell images transfected with a control plasmid.

was not present on latex-bead phagosomes in cells expressing Rab7T22N (Fig. 3b-2, b-3) (17). We also found that clustering of RILP in the perinuclear regions was disrupted and diffused by the expression of Rab7T22N. Collectively, our data demonstrate that Rab7 is vital for recruiting RILP to phagosomes during the maturation process, but not for recruiting CD63.

How *M.tb* escapes the effects of the bactericidal components within the phagosome while still acquiring nutrients for growth is very important question. It has been suggested that mycobacterial phagosomes arrest their maturation at an early stage and completely avoid fusion with lysosomes (18, 19). However, we have shown the localization of CD63 (Fig. 2) and LAMP-2 (4) on *M.tb* phagosomes in macrophages. It has been proposed that phagolysosome biogenesis is achieved by a series of fusions with heterogeneous lysosomes (20). This model is supported by a report demonstrating the existence of subpopulations of lysosomes in macrophages (6). Our previous and current studies demonstrating the alternative localization of lysosomal markers on *M.tb* phagosomes further support this model. From these observations, it seems that dissociation of Rab7 from *M.tb* phagosomes selectively inhibits fusion with harmful lysosomes despite continued fusion with non-microbicidal lysosomes.

In conclusion, based on our findings we propose the following model for *M.tb*-induced inhibition of phagolysosome biogenesis: Early *M.tb* phagosomes are capable of recruiting Rab7 and can potentially fuse with lysosomes. RILP is also recruited to *M.tb* phagosomes, which form the Rab7-RILP-dynein/dynactin protein complex followed by promotion of phagolysosome biogenesis. However, viable *M.tb* is able to release Rab7 from phagosomes, resulting in inhibition of further fusion with lysosomal vesicles and disassembly of the RILP-phagosome complex. This causes the blocking of subsequent phagolysosome biogenesis. On the other hand, non-microbicidal vesicles expressing CD63 and/or LAMP-2 continuously fuse with *M.tb* phagosomes despite Rab7 dissociation, and this fusion would support the acquisition of nutrients for mycobacterial proliferation within the phagosome.

ACKNOWLEDGMENTS

We thank Drs. Toshi Nagata and Masato Uchijima (Hamamatsu University School of Medicine, Hamamatsu, Japan) for their helpful discussion. *M.tb* strain H37Rv was kindly provided by Dr. Isamu Sugawara (Research Institute of Tuberculosis, Tokyo, Japan). This work was supported in part by Grants-in-Aid for Scientific Research from the Japan Society for the Promotion of Science, COE Research and Scientific Research on Priority Areas from the Ministry of Education, Culture, Sports, Science and Technology

of Japan, Health and Labor Science Research Grants for Research into Emerging and Reemerging Infectious Diseases from the Ministry of Health, Labor and Welfare of Japan, and the United States-Japan Cooperative Medical Science Committee.

REFERENCES

1. Armstrong J.A., Hart P.D. (1971) Response of cultured macrophages to *Mycobacterium tuberculosis*, with observations on fusion of lysosomes with phagosomes. *J Exp Med* **134**: 713–40.
2. Clemens D.L., Horwitz M.A. (1995) Characterization of the *Mycobacterium tuberculosis* phagosome and evidence that phagosomal maturation is inhibited. *J Exp Med* **181**: 257–70.
3. Van Der Wel N., Hava D., Houben D., Fluitsma D., Van Zon M., Pierson J., Brenner M., Peters P.J. (2007) *M. tuberculosis* and *M. leprae* translocate from the phagolysosome to the cytosol in myeloid cells. *Cell* **129**: 1287–98.
4. Seto S., Matsumoto S., Ohta I., Tsujimura K., Koide Y. (2009) Dissection of Rab7 localization on *Mycobacterium tuberculosis* phagosome. *Biochem Biophys Res Commun* **387**: 272–7.
5. Aoki K., Matsumoto S., Hirayama Y., Wada T., Ozeki Y., Niki M., Domenech P., Umemori K., Yamamoto S., Mineda A., Matsumoto M., Kobayashi K. (2004) Extracellular mycobacterial DNA-binding protein 1 participates in mycobacterium-lung epithelial cell interaction through hyaluronic acid. *J Biol Chem* **279**: 39798–806.
6. Astarie-Dequeker C., Carreno S., Cougoule C., Maridonneau-Parini I. (2002) The protein tyrosine kinase Hck is located on lysosomal vesicles that are physically and functionally distinct from CD63-positive lysosomes in human macrophages. *J Cell Sci* **115**: 81–9.
7. Fratti R.A., Chua J., Deretic V. (2003) Induction of p38 mitogen-activated protein kinase reduces early endosome auto-antigen 1 (EEA1) recruitment to phagosomal membranes. *J Biol Chem* **278**: 46961–7.
8. Nieuwenhuis H.K., Van Oosterhout J.J., Rozemuller E., Van Iwaarden F., Sixma J.J. (1987) Studies with a monoclonal antibody against activated platelets: evidence that a secreted 53 000-molecular weight lysosome-like granule protein is exposed on the surface of activated platelets in the circulation. *Blood* **70**: 838–45.
9. Bampton E.T., Goemans C.G., Niranjan D., Mizushima N., Tolkovsky A.M. (2005) The dynamics of autophagy visualized in live cells: from autophagosome formation to fusion with endo/lysosomes. *Autophagy* **1**: 23–36.
10. Fukuda M. (1991) Lysosomal membrane glycoproteins: structure, biosynthesis, and intracellular trafficking. *J Biol Chem* **266**: 21327–30.
11. Metzelaar M.J., Wijngaard P.L., Peters P.J., Sixma J.J., Nieuwenhuis H.K., Clevers H.C. (1991) CD63 antigen. A novel lysosomal membrane glycoprotein cloned by a screening procedure for intracellular antigens in eukaryotic cells. *J Biol Chem* **266**: 3239–45.
12. Artavanis-Tsakonas K., Love J.C., Ploegh H.L., Vyas J.M. (2006) Recruitment of CD63 to *Cryptococcus neoformans* phagosomes requires acidification. *Proc Natl Acad Sci U S A* **103**: 15945–50.
13. Beatty W.L., Rhoades E.R., Hsu D.K., Liu F.T., Russell D.G. (2002) Association of a macrophage galactoside-binding protein with Mycobacterium-containing phagosomes. *Cell Microbiol* **4**: 167–76.
14. Cantalupo G., Alifano P., Roberti V., Bruni C.B., Bucci C. (2001) Rab-interacting lysosomal protein (RILP): the Rab7 effector required for transport to lysosomes. *Embo J* **20**: 683–93.
15. Jordens I., Fernandez-Borja M., Marsman M., Dusseljee S., Janssen L., Calafat J., Janssen H., Wubbolts R., Neefjes J. (2001) The Rab7 effector protein RILP controls lysosomal transport by inducing the recruitment of dynein-dynactin motors. *Curr Biol* **11**: 1680–5.
16. Harrison R.E., Bucci C., Vieira O.V., Schroer T.A., Grinstein S. (2003) Phagosomes fuse with late endosomes and/or lysosomes by extension of membrane protrusions along microtubules: role of Rab7 and RILP. *Mol Cell Biol* **23**: 6494–506.
17. Sun J., Deghmane A.E., Soualhine H., Hong T., Bucci C., Solodkin A., Hmama Z. (2007) *Mycobacterium bovis* BCG disrupts the interaction of Rab7 with RILP contributing to inhibition of phagosome maturation. *J Leukoc Biol* **82**: 1437–45.
18. Deretic V., Singh S., Master S., Harris J., Roberts E., Kyei G., Davis A., De Haro S., Naylor J., Lee H.H., Vergne I. (2006) *Mycobacterium tuberculosis* inhibition of phagolysosome biogenesis and autophagy as a host defence mechanism. *Cell Microbiol* **8**: 719–27.
19. Deretic V., Vergne I., Chua J., Master S., Singh S.B., Fazio J.A., Kyei G. (2004) Endosomal membrane traffic: convergence point targeted by *Mycobacterium tuberculosis* and HIV. *Cell Microbiol* **6**: 999–1009.
20. Rohde K., Yates R.M., Purdy G.E., Russell D.G. (2007) *Mycobacterium tuberculosis* and the environment within the phagosome. *Immunol Rev* **219**: 37–54.

THE JOURNAL OF BIOLOGICAL CHEMISTRY VOL. 285, NO. 18, pp. 13326–13336, April 30, 2010

Controlled Expression of Branch-forming Mannosyltransferase Is Critical for Mycobacterial Lipoarabinomannan Biosynthesis[S]

Received for publication, October 21, 2009, and in revised form, February 12, 2010 Published, JBC Papers in Press, March 9, 2010, DOI 10.1074/jbc.M109.077297

Chubert B. C. Sena[‡], Takeshi Fukuda[‡], Kana Miyanagi[‡], Sohkichi Matsumoto[§1], Kazuo Kobayashi[¶1], Yoshiko Murakami[‡], Yusuke Maeda[‡], Taroh Kinoshita[‡2], and Yasu S. Morita[‡3]

From the [‡]Research Institute for Microbial Diseases and WPI-Immunology Frontier Research Center, Osaka University, Osaka 565-0871, Japan, the [§]Department of Bacteriology, Osaka City University Graduate School of Medicine, Osaka 545-8585, Japan, and the [¶]Department of Immunology, National Institute of Infectious Diseases, Tokyo 162-8640, Japan

Lipomannan (LM) and lipoarabinomannan (LAM) are phosphatidylinositol-anchored glycans present in the mycobacterial cell wall. In *Mycobacterium smegmatis*, the mannan core of LM/LAM constitutes a linear chain of 20–25 α1,6-mannoses elaborated by 8–9 α1,2-monomannose side branches. At least two α1,6-mannosyltransferases mediate the linear mannose chain elongation, and one branching α1,2-mannosyltransferase (encoded by *MSMEG_4247*) transfers monomannose branches. An *MSMEG_4247* deletion mutant accumulates branchless LAM and interestingly fails to accumulate LM, suggesting an unexpected role of mannose branching for LM synthesis or maintenance. To understand the roles of MSMEG_4247-mediated branching more clearly, we analyzed the *MSMEG_4247* deletion mutant in detail. Our study showed that the deletion mutant restored the synthesis of wild-type LM and LAM upon the expression of MSMEG_4247 at wild-type levels. In striking contrast, overexpression of MSMEG_4247 resulted in the accumulation of dwarfed LM/LAM, although monomannose branching was restored. The dwarfed LAM carried a mannan chain less than half the length of wild-type LAM and was elaborated by an arabinan that was about 4 times smaller. Induced overexpression of an elongating α1,6-mannosyltransferase competed with the overexpressed branching enzyme, alleviating the dwarfing effect of the branching enzyme. In wild-type cells, LM and LAM decreased in quantity in the stationary phase, and the expression levels of branching and elongating mannosyltransferases were reduced in concert, presumably to avoid producing abnormal LM/LAM. These data suggest that the coordinated expressions of branching and elongating mannosyltransferases are critical for mannan backbone elongation.

Mycobacterium tuberculosis is an etiologic agent of tuberculosis, an infectious disease that remains a global problem. Glycoconjugates from the mycobacterial cell wall are involved in pathogenesis and immune modulation. In particular, phosphatidylinositol mannosides (PIMs),[4] lipomannan (LM), and lipoarabinomannan (LAM) form a class of glycoconjugates found in all species of mycobacteria, including pathogenic *M. tuberculosis* and saprophytic and experimentally tractable *Mycobacterium smegmatis*, and are known to have potent immunomodulatory activities (1–3). PIMs are anchored to the plasma membrane by a phosphatidylinositol (PI) and carry two or six mannoses, which are directly linked to the 2-OH and 6-OH of the inositol residue (4, 5) (Fig. 1*A*). Monomannose attached to the 2-OH of inositol is further modified by a fatty acid, making triacylated PIMs the major lipid species. The 3-OH of inositol can be further modified by a fatty acid to become a tetra-acylated species (6). LM carries a much longer chain of mannoses. For example, in *M. smegmatis*, 20–25 α1,6-mannose residues were thought to form a linear chain, which is elaborated by 8–9 α1,2-mannose monomer branches (7). A more recent report estimated *M. smegmatis* LM to carry 21–34 mannose residues (8), highlighting even greater heterogeneity of this molecule. LAM is an arabinosylated LM, in which ~70 residues of D-arabinofuranose form arabinan(s) comprising α1,5 linear stretches linked by multiple α1,3 branch points (9, 10). It is not known if a single molecule of LAM carries a single large arabinan moiety or multiple smaller arabinans.

PIMs, LM, and LAM all contain PI as a common lipid core moiety and are thought to be biosynthesized in a sequential order. PIMs are synthesized from a PI by sequential additions of mannoses, resulting in dimannosyl or hexamannosyl PIMs (6, 11–13). PimA and PimB′ mediate the transfers of first two mannoses in a GDP-mannose-dependent manner, and an acyltransferase, encoded by *MSMEG_2934* in *M. smegmatis*, adds one fatty acid onto a mannose residue to produce a dimannosyl species, AcPIM2 (14–16). Then, an additional four mannose residues are transferred onto AcPIM2, producing AcPIM6.

[S] The on-line version of this article (available at http://www.jbc.org) contains supplemental Table S1 and Figs. S1–S5.

[1] Supported by grants from the Ministry of Health, Labor, and Welfare (Research on Emerging and Re-emerging Infectious Diseases), Ministry of Education, Culture, Sports, Science, and Technology, Japan Health Sciences Foundation, and the United States-Japan Cooperative Medical Science Program against Tuberculosis and Leprosy.

[2] Supported by the Knowledge Cluster Initiative of the Ministry of Education, Culture, Sports, Science, and Technology.

[3] Supported by grants from the International Human Frontier Science Program and Japan Society for the Promotion of Science (KAKENHI 20590441).
To whom correspondence should be addressed: Dept. of Immunoregulation, Research Institute for Microbial Diseases, Osaka University, 3-1 Yamada-oka, Suita, Osaka 565-0871, Japan. Tel.: 81-6-6879-8329; Fax: 81-6-6875-5233; E-mail: ymorita@biken.osaka-u.ac.jp.

[4] The abbreviations used are: PIM, phosphatidylinositol mannoside; HPAEC, high performance anion exchange chromatography; HPTLC, high performance thin layer chromatography; LAM, lipoarabinomannan; LM, lipomannan; PI, phosphatidylinositol; Tricine, *N*-[2-hydroxy-1,1-bis(hydroxymethyl)ethyl]glycine.

Polyprenol-phosphate-mannose-dependent mannosyltransferases are thought to be involved in these later reactions (11, 13), but only the fifth mannosyltransferase, PimE, has so far been identified (17). AcPIM4 has been thought to be the branching point from which LM/LAM biosynthesis diverges from the PIM biosynthetic pathway, and a lipoprotein, LpqW, is thought to be involved in controlling the metabolic flux at this branch point (18, 19). This branch point is structurally viable because the terminal two mannoses of AcPIM6 are α1,2-linked, whereas the LM/LAM mannan chain is α1,6-linked. LM is believed to be the precursor of LAM, but the precursor-product relationship has not been experimentally proven.

The linear α1,6-mannose chain of LM is synthesized by an α1,6-mannosyltransferase encoded by *MSMEG_4241* in *M. smegmatis* (8) or MptA in a related organism, *Corynebacterium glutamicum* (20). Deletion of *MSMEG_4241* results in the accumulation of an intermediate containing 5–20 mannose residues instead of mature LM containing 21–34 mannose residues (Fig. 1*A*). Accumulation of the LM_{5-20} intermediate suggests that there is another α1,6-mannosyltransferase that mediates the initial stage of LM synthesis up to LM_{5-20}. Another gene, *MSMEG_3111*, might potentially play a role in LM/LAM biosynthesis because it is homologous to an α1,6-mannosyltransferase of *Corynebacterium* LM (21). However, an *MSMEG_3111* gene deletion mutant showed no defects in LM/LAM production (21), leaving its precise function unclear.

MSMEG_4247 and its *M. tuberculosis* ortholog, Rv2181, are α1,2-mannosyltransferases involved in LM/LAM biosynthesis (22, 23). An *MSMEG_4247* gene deletion mutant produced LAM lacking the α1,2-monomannose side chains, suggesting that MSMEG_4247 is responsible for the addition of the α1,2-mannose branches onto the α1,6-mannose backbone of LAM. Interestingly, the *MSMEG_4247* gene deletion mutant failed to accumulate LM (22), suggesting an essential role for the α1,2-mannose branch in the accumulation of LM.

A number of mannosyltransferases involved in the PIM/LM/LAM biosynthetic pathway have now been identified, but it remains largely unknown how these enzymes coordinate and control the complex and overlapping pathways of PIM/LM/LAM synthesis. As part of our study of the *pimE* gene (17), we generated an *MSMEG_4247* gene deletion mutant. Here we report our analyses on the Δ*MSMEG_4247* mutant, revealing that controlling expression levels of MSMEG_4247 is critical for the proper synthesis of LM and LAM.

EXPERIMENTAL PROCEDURES

Mycobacterial Strains and Culture Conditions—Wild-type *M. smegmatis* strain mc^2155 (24) and derived mutants were grown at 30 °C in Middlebrook 7H9 broth (BD Biosciences) supplemented with 0.2% (w/v) glucose, 0.2% (v/v) glycerol, 15 mM NaCl, and 0.05% (v/v) Tween 80. Where appropriate, antibiotics at the following concentrations were used: 20 μg/ml streptomycin, 200 μg/ml hygromycin, or 20 μg/ml kanamycin. Samples were prepared at logarithmic growth phase (A_{600} nm = 0.5–1.0) unless otherwise indicated.

Gene Cloning and Complementation—A fragment containing the *MSMEG_4247* gene was PCR-amplified (primers 053/054; supplemental Table S1) from *M. smegmatis* genomic DNA and cloned into the MscI and EcoRI sites of the episomal expression vector, pHBJ334 (25), driven by a strong promoter of a mycobacterial heat shock protein hsp60 (Phsp60), resulting in pYAB143. To create an integrative vector, an XbaI/SpeI fragment of pYAB143, containing Phsp60, the *MSMEG_4247* gene, and the streptomycin resistance cassette, was blunt end-ligated with an SpeI/Eam1105I fragment of pMV361 (26), containing the attachment site and integrase gene, resulting in pYAB243. Site-directed mutagenesis was performed as described previously (17), using pYAB143 or pYAB250 as a template and primers 320/321, resulting in pYAB254 or pYAB255. Hygromycin-resistant versions of the expression vectors were constructed as follows: pYAB251 by replacing the streptomycin resistance cassette of pHBJ334, pYAB250 by replacing the streptomycin resistance cassette of pYAB143, and pYAB184 by replacing the kanamycin resistance cassette of pMV306 (26). For an expression vector driven by the endogenous promoter, the *MSMEG_4247* gene and 200 bp of upstream flanking sequence was PCR-amplified (primers 312/313) and ligated into the ClaI/XbaI sites of pYAB184, resulting in pYAB247. For the acetamide-inducible system, the *MSMEG_4241* gene was PCR-amplified (primers 329/330) and ligated into the BamHI/XbaI sites of pJAM2 (27), resulting in pYAB262. To make an acetamide-inducible MSMEG_4247 expression vector (pYAB246), the kanamycin resistance cassette of pJAM2 was first replaced by a streptomycin resistance cassette, resulting in pYAB040, and the HindIII/Bpu1102I fragment of pYAB143 containing the *MSMEG_4247* gene was blunt end-ligated into the BamHI site of pYAB040. These constructs were transfected into *M. smegmatis* wild-type strain mc^2155 and mutant cells by electroporation.

Lipid Extraction and Analysis—The cell wall lipids were extracted from the cell pellets as described previously (17). Extracted lipids were analyzed by high performance thin layer chromatography (HPTLC) using chloroform, methanol, 13 M ammonia, 1 M ammonium acetate, water (180:140:9:9:23, v/v/v/v/v) as a solvent. Orcinol or molybdenum blue staining was used to visualize PIMs or phospholipids, respectively.

LM and LAM Extraction and Analysis—After lipid extraction, the delipidated pellets were resuspended in five volumes of phenol saturated with Tris-EDTA buffer (pH 6.6) (Nacalai Tesque, Kyoto, Japan) and five volumes of water and extracted for 2 h at 55 °C. The extract was further purified by dialysis or octyl-Sepharose column chromatography (GE Healthcare) and electroelution (model 422 Electro-Eluter, Bio-Rad) from an SDS-polyacrylamide gel where appropriate. LM/LAM were separated by SDS-PAGE (10–20% gradient gel) and visualized using the ProQ Emerald 488 carbohydrate staining kit (Molecular Probes) and a fluoroimage analyzer (FLA-5000, Fujifilm).

*Metabolic Labeling of Δ*MSMEG_4247*—Cells were washed and resuspended in a fresh aliquot of Middlebrook 7H9 broth at 0.2 g/ml pellet. Cells were radiolabeled with 50 μCi/ml D-[2-^{3}H]mannose (20 Ci/mmol; American Radiolabeled Chemicals) for 15 min, washed in 7H9 broth to remove unincorporated radioactive mannose, and chased in 7H9 broth containing 1 mM

mannose. Extracted LM/LAM were separated by SDS-PAGE and visualized by fluorography.

Mannosidase Treatment—LM/LAM fractions, mixed with PIMs as internal controls, were treated with or without 0.4 milliunits of *Aspergillus saitoi* α1,2-mannosidase (Prozyme) for 24 h at 37 °C. The treatment was repeated three times. LM/LAM were repurified by phenol and analyzed by SDS-PAGE as described above. Intensity profiles were obtained by the Multi Gauge software (Fujifilm). PIMs were purified by 1-butanol/water (2:1, v/v) partitioning and analyzed by HPTLC.

High Performance Anion Exchange Chromatography (HPAEC)—Acetolysis was performed following a published protocol (28). Monosaccharides were released by 2 M trifluoroacetic acid at 100 °C for 2 h. Released carbohydrates were analyzed by a Nanospace high performance liquid chromatography system (Shiseido, Tokyo, Japan) equipped with Screbead II (2.0 × 250 mm) (Shiseido) as an anion exchange column, 50 mM sodium acetate in 0.1 M NaOH as a mobile phase, and a pulsed amperometric detector.

Western Blotting—Rabbit antibodies were raised against a mixture of two peptides from MSMEG_4241 (MTPTETHK-PNPGLAEHVC and CRAPESAEATASRQ), MSMEG_4247 (RTHTGDAHETDEPLVPLC and MSKRQSPRGAGLAPC), or PimB′ (CEHLPPGVDTDRFAPDPD and CGARLAELLSGRR-EARQA) and affinity-purified. Cell lysates were prepared by bead beating as described previously (17). Proteins were fractionated by SDS-PAGE (10–20% gradient gel) under reducing conditions and blotted onto a polyvinylidene difluoride membrane (Millipore). The membrane was blocked with 5% skim milk and then incubated with a primary antibody (rabbit anti-MSMEG_4247, anti-MSMEG_4241, or anti-PimB′ antibodies; 1 μg/ml) for 1 h and a secondary antibody (anti-rabbit IgG antibody, horseradish peroxidase-conjugated; 1:2000 dilution; Amersham Biosciences) for 1 h. The bound probe was visualized by chemiluminescence (PerkinElmer Life Sciences). Images were captured by a luminescent image analyzer (LAS-4000, Fujifilm) and quantified by the Multi Gauge software.

Acetamide-induced Expression and Metabolic Labeling—Cells were grown in Middlebrook 7H9 medium, and 0.2% acetamide was added at midlog phase. After induction, the cells were washed in Sauton's medium (29), resuspended at 0.2 g/ml pellet, pulse-labeled with D-[2-^{3}H]mannose (24.7 Ci/mmol; PerkinElmer Life Sciences) for 15 min, and diluted 50-fold in Middlebrook 7H9 broth containing 1 mM mannose for chase. Extracted LM/LAM were separated by SDS-PAGE and visualized by fluorography.

Subcellular Fractionation—Cells were lysed by nitrogen cavitation, and the crude lysate was separated by a sucrose density gradient (25–56%) as described previously (30). Each fraction was tested for protein concentration, PIM biosynthetic activities (30), and Western blot detection of MSMEG_4247, MSMEG_4241, and PimB′.

RESULTS

Complementation of MSMEG_4247-deficient Mutant with MSMEG_4247 Does Not Restore the Synthesis of Normal LM and LAM—We deleted the *MSMEG_4247* gene by homologous recombination and confirmed the gene deletion by Southern blotting (supplemental Fig. S1, *A* and *B*). We extracted LM and LAM from the deletion mutant and analyzed them by SDS-PAGE. We found even greater accumulation of LAM in the Δ*MSMEG_4247* mutant, but the mutant LAM appeared slightly smaller than that from wild type. More striking, the mutant lacked LM completely (Fig. 1*B*; wild type (*lanes 1–3*) and Δ*MSMEG_4247* (*lanes 4–6*)), as reported recently (see Fig. 2 of Ref. 22). The complete disappearance of LM was unexpected because the lack of the α1,2 side chain should still leave the α1,6 backbone intact. We considered the possibility that LM was synthesized but could not accumulate. To test this possibility, we radiolabeled the Δ*MSMEG_4247* mutant metabolically in a pulse-chase experiment using [^{3}H]mannose. The mutant cells produced a weakly radiolabeled species (Fig. 1*C*, *asterisk*), which had an electrophoretic mobility similar to that of wild-type LM. The radiolabeled LM in the wild-type cells remained during the 5-h chase period, whereas the mutant LM completely disappeared within 5 h, suggesting that LM could only accumulate transiently in the mutant. We next examined whether these phenotypes were rescued by the introduction of the MSMEG_4247 expression vector. We used an episomal expression vector, in which a strong hsp60

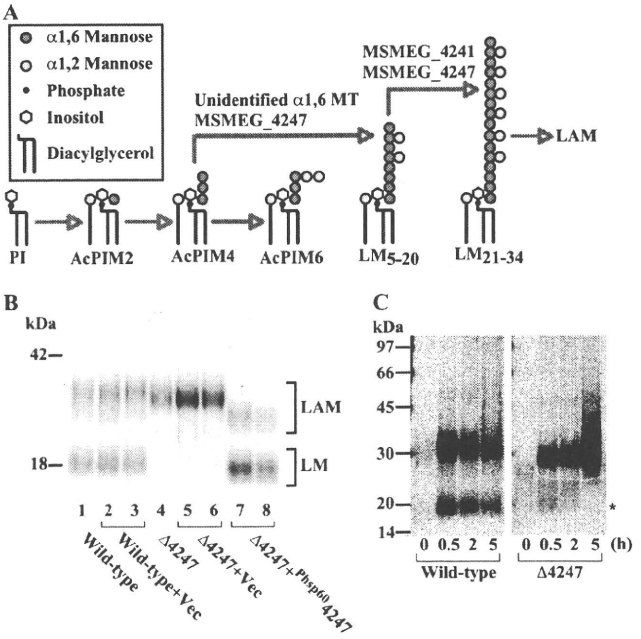

FIGURE 1. **The phenotype of *MSMEG_4247* deletion mutant (Δ*MSMEG_4247*) cannot be restored by introduction of the episomal MSMEG_4247 overexpression vector.** *A*, proposed pathway of PIM, LM, and LAM biosynthesis. Note that AcPIM4 is a proposed branch point from which the LM/LAM biosynthesis pathways diverge. The mannosyltransferase (*MT*) that mediates the initial elongation of the α1,6-mannose chain to produce LM_{5-20} has not been identified. The positions of the α1,2 side branches are hypothetical. Only the products and key intermediates are shown, and tetra-acylated PIMs are not shown for simplicity. *B*, LM/LAM from Δ*MSMEG_4247* and its complemented strains were analyzed by SDS-PAGE and visualized by carbohydrate staining. Wild-type (*lanes 1–3*) and Δ*MSMEG_4247* mutant (*lanes 4–8*) were transfected with an empty vector (*lanes 2, 3, 5,* and *6*, pYAB251) or an episomal ^{Phsp60}*MSMEG_4247* vector (*lanes 7* and *8*, pYAB250). Loading was adjusted for equal cell pellet equivalents. *C*, [^{3}H]mannose metabolic labeling of LM and LAM in the Δ*MSMEG_4247* mutant strain. Cells were pulsed with [^{3}H]mannose for 15 min and chased with excess non-radioactive mannose for up to 5 h. LM and LAM profiles were analyzed by SDS-PAGE and fluorography. Transient synthesis of LM is indicated by an *asterisk*.

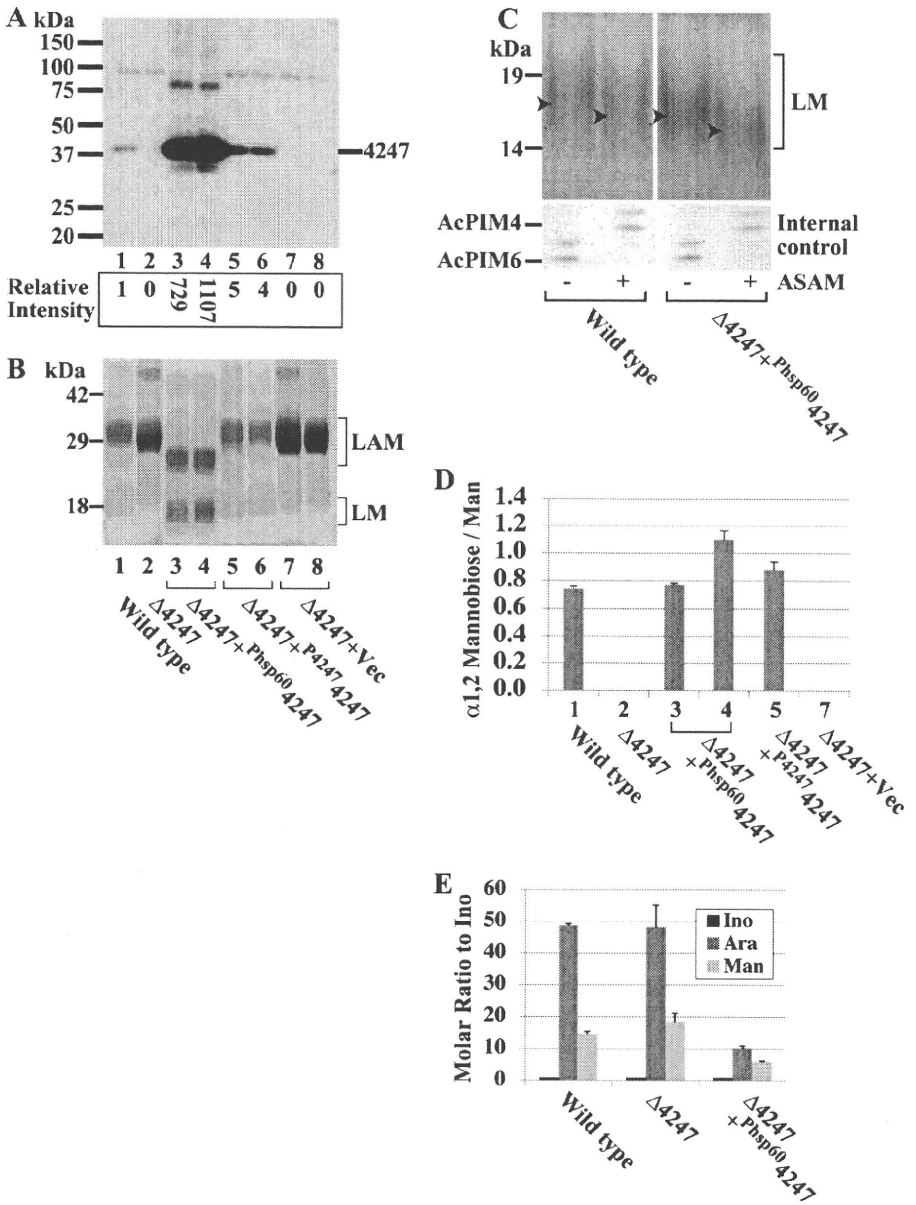

FIGURE 2. **Controlled expression of MSMEG_4247 is critical for the restoration of LM/LAM biosynthesis.** *A*, MSMEG_4247 expression examined by Western blotting using anti-MSMEG_4247 antibody. *Lane 1*, wild type; *lane 2*, Δ*MSMEG_4247*; *lanes 3* and *4*, two clones of Δ*MSMEG_4247*+^{Phsp60}*MSMEG_4247* (pYAB250); *lanes 5* and *6*, two clones of Δ*MSMEG_4247*+^{P4247}*MSMEG_4247* (pYAB247); *lanes 7* and *8*, two clones of Δ*MSMEG_4247* transfected with empty integrative vector (pYAB184). Loading was adjusted to 5 μg of protein/lane except for *lanes 3* and *4*, in which 1 μg of protein was loaded per lane. Relative intensities were calculated taking different protein loadings into account. *B*, LM/LAM profiles of *MSMEG_4247* deletion mutants complemented by various expression vectors. LM/LAM were analyzed by SDS-PAGE and visualized by carbohydrate staining. Lanes are arranged in the same order as in *A*. Faint doublet bands slightly above the 18 kDa marker seen in all *lanes* are protein contaminants. *C*, LM from wild-type or Δ*MSMEG_4247*+^{Phsp60}*MSMEG_4247* was treated with or without α1,2-mannosidase (*ASAM*), analyzed by SDS-PAGE using Tris-Tricine gel (15–20%) to improve the separation, and visualized by carbohydrate staining. Peak of LM in each *lane* was determined from the intensity profile and is indicated by an *arrowhead*. PIMs were included as internal controls and showed specific and complete digestion of the terminal two α1,2-mannoses of AcPIM6, producing AcPIM4. *D*, LM/LAM extracts were acetolyzed, and released mannose and α1,2-mannobiose were detected by HPAEC. Molar ratios of α1,2-mannobiose to mannose, measured in triplicate, are shown as averages with S.D. values. *Column numbers* specify the samples analyzed in the corresponding *lanes* in *A* and *B*. *E*, LAM was purified by electroelution and hydrolyzed by 2 M trifluoroacetic acid. Released carbohydrates were quantified by HPAEC. Data are presented as molar ratio relative to inositol. Averages of triplicate measurements with S.D. values are shown.

promoter (Phsp60) regulates the expression of MSMEG_4247 (26). Strikingly, the rescued mutant (Δ*MSMEG_4247*+^{Phsp60}*MSMEG_4247*) produced LM and LAM, but they were both smaller than those produced by the wild type (Fig. 1*B*, *lanes 7* and *8*).

Expression Level of MSMEG_4247 Is Critical for Controlling the Sizes of LM and LAM Produced—We considered the possibility that LM/LAM synthesis was prematurely terminated because of the high expression level of MSMEG_4247. We found that Δ*MSMEG_4247*+^{Phsp60}*MSMEG_4247* expressed MSMEG_4247 at >700 times the levels of the wild-type (Fig. 2*A*, compare *lanes 1* and *lanes 3* and *4*; note that the protein loading is 5 times less in *lanes 3* and *4*). To achieve a more controlled expression of MSMEG_4247, the Δ*MSMEG_4247* mutant was transfected with a vector carrying *MSMEG_4247* with its own upstream region instead of an artificial promoter. This vector lacks the mycobacterial origin of replication and instead carries the attachment site and the integrase gene from the mycobacteriophage L5, allowing for the site-specific integration of a single copy of the *MSMEG_4247* gene (26). Western blotting confirmed that the expression levels of MSMEG_4247 in the complemented strains (Δ*MSMEG_4247*+^{P4247}*MSMEG_4247*) were much closer to those of wild-type (4–5-fold overexpression; Fig. 2*A*, compare *lane 1* and *lanes 5* and *6*). As shown in Fig. 2*B*, LM and LAM from Δ*MSMEG_4247*+^{P4247}*MSMEG_4247* restored the migration pattern of wild-type LM and LAM (*lanes 5* and *6*). In contrast, Δ*MSMEG_4247*+^{Phsp60}*MSMEG_4247* reproducibly accumulated faster migrating LM and LAM (*lanes 3* and *4*). These results suggest that the sizes of LM and LAM are normalized if the Δ*MSMEG_4247* mutant is complemented with a wild-type level of MSMEG_4247 expression.

MSMEG_4247 is an α1,2-mannosyltransferase involved in the

transfer of the monomannose side chain. It was therefore perplexing that its overexpression resulted in smaller LM and LAM. To investigate whether the smaller sized LM and LAM produced in MSMEG_4247-overexpressing strains were modified by α1,2-mannose side chains, we removed the α1,2-mannose branches of LM by α1,2-specific mannosidase treatment and analyzed the size changes by SDS-PAGE (Fig. 2*C*). A shift of LM was detectable upon digestion of LM from both the wild-type and overexpressing strains. To confirm further, we acetolyzed the LM/LAM mixture from select strains and quantified the frequencies of α1,2-mannose branching. Acetolysis cleaves α1,6-mannose linkages without digesting α1,2-mannose linkages, producing α1,2-mannobiose and mannose. The ratio of α1,2-mannobiose to mannose indicates the ratio of mannoses with α1,2-mannose branches to those without. As shown in Fig. 2*D*, whereas the Δ*MSMEG_4247* mutant completely lacked the α1,2-mannose branch, LM/LAM from all complemented strains showed frequencies of α1,2-mannose branches comparable with those of the wild-type LM/LAM (*i.e.* ~45–50% of backbone mannoses were branched).

Despite the restoration of α1,2-mannose branching, LM and LAM from the Δ*MSMEG_4247*+^{Phsp60}*MSMEG_4247* strain appeared small on SDS-PAGE. To determine which component of LAM was responsible for the SDS-PAGE mobility shift, we purified LAM from an SDS-polyacrylamide gel by electroelution and analyzed its sugar composition. As shown in Fig. 2*E*, the Δ*MSMEG_4247* mutant did not show significant changes in the sugar compositions of LAM despite the lack of α1,2-mannose branches, suggesting that α1,6-mannose backbone is longer than that of wild-type LAM, and arabinosylation is occurring normally. The numbers of arabinose and mannose residues relative to inositol were somewhat smaller than previously reported (~70 arabinose and 21–34 mannose residues; see Introduction). This might be due to the contribution of inositol from inositol phosphate capping, a minor modification of LAM arabinan in *M. smegmatis* and other fast growing mycobacteria (31, 32). Strikingly, LAM from the Δ*MSMEG_4247*+^{Phsp60}*MSMEG_4247* strain showed greatly reduced numbers of arabinose and mannose. The mannan core carried less than half the number of mannose residues found in wild-type LAM. Because the frequency of the side-chain mannose is not significantly different between the dwarfed and wild-type LAM, these data suggest that the length of mannan backbone is less than half the length of wild-type LAM. Furthermore, arabinan was found to be 4 times smaller. This gross dwarfing is apparently the cause of faster migration on the SDS-polyacrylamide gel, although the protein molecular weight standards do not precisely reflect the actual molecular weight shifts of LM/LAM (see also Ref. 33 for another example). Taken together, our data suggested that overexpression of MSMEG_4247 restored the branches of α1,2-monomannose but prematurely terminated the elongation of the α1,6-mannose backbone and dwarfed the arabinan size.

Next we investigated whether the effect of MSMEG_4247 overexpression is specific to the LM/LAM pathway. Because LM/LAM biosynthetic pathways are thought to diverge from PIM biosynthesis at the AcPIM4 intermediate (see Fig. 1*A*), we examined the lipid fractions to see if there are any changes in the PIM or phospholipid profiles. We found no significant differences in either PIMs or phospholipids (supplemental Fig. S2), suggesting that the deletion or overexpression of MSMEG_4247 primarily affects LM/LAM biosynthesis.

Dwarfing LM/LAM Requires and Correlates with MSMEG_4247 Enzyme Activity—If the expression levels of MSMEG_4247 affect the elongation of the α1,6-mannose backbone, overexpression of MSMEG_4247 can affect the profile of LM and LAM in wild-type cells as well. To test this prediction, we introduced integrative or episomal MSMEG_4247 overexpression vectors and examined the effect of expression in the wild-type cells. Indeed, overexpression of MSMEG_4247 resulted in smaller LM and LAM in wild-type cells (Fig. 3*A*). A higher expression level was achieved using an episomal vector compared with an integrative vector. The hyperexpression in cells transfected with the episomal vector led to the production of LM and LAM, which appeared even smaller than the LM and LAM from cells transfected with the integrative vector (Fig. 3*A*, compare *lane 2* with *lanes 3* and *4*). To examine whether the production of smaller LM and LAM was dependent on the enzyme activity of MSMEG_4247, we created an MSMEG_4247 expression vector, in which the gene carried a site-directed mutation at a conserved aspartic acid residue. The aspartic acid residue 45 was conserved among mycobacterial species and aligned with the aspartic acid residue of PimE that is essential for enzymatic activity (supplemental Fig. S3*A*) (17). The expression of D45A-mutated MSMEG_4247 could not alter the LM/LAM profile of the Δ*MSMEG_4247* mutant, suggesting the loss of enzyme activity (supplemental Fig. S3, *B* and *C*). When introduced in the wild-type cells, the D45A mutant of MSMEG_4247 did not show a shift in the migration patterns of wild-type LM and LAM (Fig. 3*A*, *lanes 5* and *6*). The lack of effect was not due to the lack of expression of MSMEG_4247 D45A mutant because it was expressed at a level comparable with that of wild-type MSMEG_4247 (Fig. 3*B*, compare *lane 2* with *lanes 5* and *6*). These data further support our notion that the enzyme activity of MSMEG_4247 needs to be properly controlled to produce normal sized LM and LAM.

LM/LAM Biosynthesis Is Immediately Affected by Induced Expression of MSMEG_4247—Secondary mutations sometimes occur to compensate for an existing mutation in the genome, and secondary mutants with improved growth fitness can outgrow the original mutant. For example, deletion of the *lpqW* gene leads to spontaneous mutations in the *pimE* gene, resulting in an improved growth fitness of the mutant (18). We therefore wanted to exclude the possibility that the constitutive overexpression of MSMEG_4247 resulted in secondary mutations and that smaller LM/LAM was the consequence of these secondary mutations. To address this possibility, we created a vector, in which MSMEG_4247 expression was controlled by an acetamide-inducible promoter (27) and introduced this vector into wild-type cells. As shown in Fig. 4*A*, the acetamide-inducible promoter is leaky and expresses MSMEG_4247 at a level significantly higher than the wild-type level (compare *lanes 1* and *3*). Nevertheless, a much higher expression level was achieved after 4 h of acetamide induction (*lane 6*). At the 4-h time point, cells were metabolically pulse-

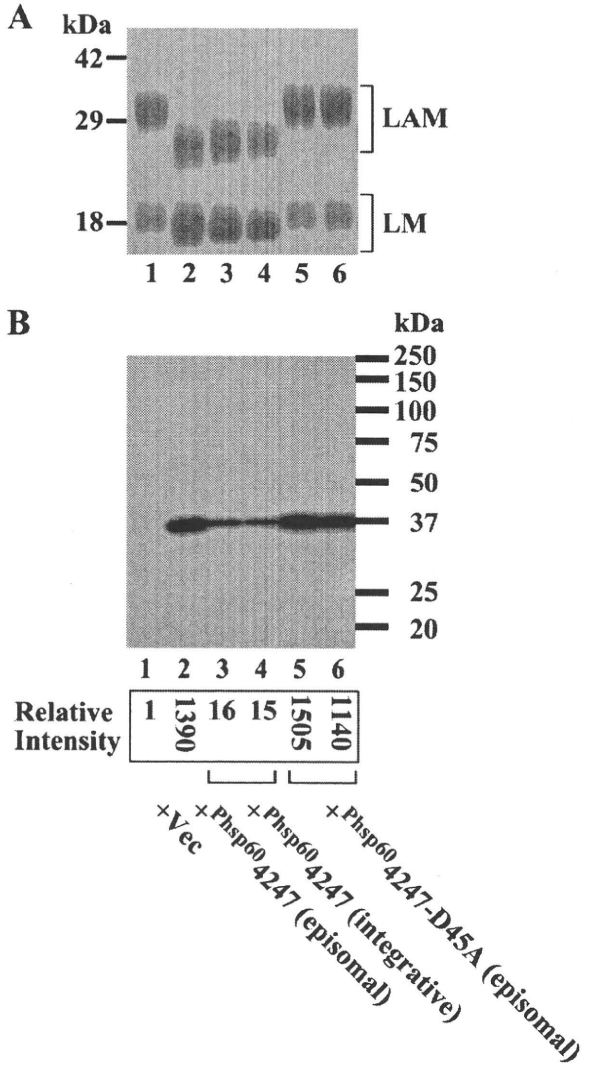

FIGURE 3. **Overexpression of MSMEG_4247 reduces the sizes of LM and LAM in wild-type cells.** *A*, LM/LAM profiles of wild-type cells transfected with various Phsp60-driven expression vectors were analyzed by SDS-PAGE and visualized by carbohydrate staining. *Lane 1*, empty vector (pHBJ334); *lane 2*, episomal vector to express MSMEG_4247 (pYAB143); *lanes 3* and *4*, integrative vector to express MSMEG_4247 (pYAB243); *lanes 5* and *6*, episomal vector to express MSMEG_4247 D45A mutant (pYAB254). *B*, MSMEG_4247 expression examined by Western blotting using anti-MSMEG_4247 antibody. *Lanes* are arranged in the same order as in *A*. Loading was adjusted to 5 μg of protein/lane for *lanes 1*, *3*, and *4* or 0.25 μg/lane for *lanes 2*, *5*, and *6*. Relative intensities were calculated, taking different protein loadings into account.

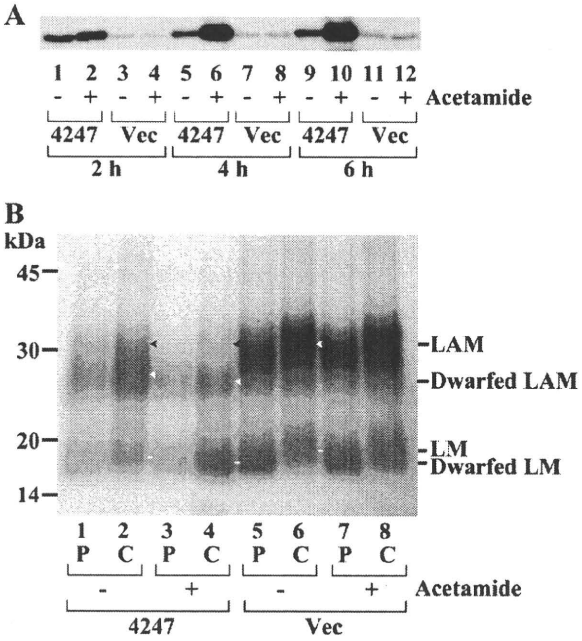

FIGURE 4. **Acetamide-induced overexpression of MSMEG_4247 prevents the maturation of LM/LAM.** *A*, acetamide induction of MSMEG_4247 examined by Western blotting using anti-MSMEG_4247 antibody. Wild-type cells transfected with either the acetamide-inducible MSMEG_4247 expression vector (*4247*) (transfected with pYAB246) or empty vector (*Vec*) (transfected with pYAB040) were incubated with (+) or without (−) acetamide for the indicated period to induce MSMEG_4247 expression. *B*, metabolic labeling with [^{3}H]mannose. Cells were incubated with (+) or without (−) acetamide for 4 h prior to radiolabeling. Cells were pulsed (*P*) for 15 min and then chased (*C*) in the presence of excess non-radioactive mannose for 25 min. The *white arrowheads* and *lines* indicate the peaks of LAM and LM, respectively, in *lanes 2*, *4*, and *6*, as determined by the intensity profiles shown in supplemental Fig. S4. The *black arrowheads* indicate the position of normal LAM as determined by the *white arrowhead* in *lane 6*.

labeled with [^{3}H]mannose and chased for 25 min in the presence of excess non-radioactive mannose (Fig. 4*B*). LM and LAM were relatively small in size immediately after pulse (*lanes* designated *P*). After the chase (*lanes* designated *C*), increased LM/LAM sizes were detected in control strains (compare *lanes 5* and *6* or *lanes 7* and *8*). Compared with control strains, the sizes of LM and LAM after chase remained smaller in the cells carrying acetamide-inducible MSMEG_4247 even without acetamide induction due to leaky expression of MSMEG_4247 (compare *lanes 2* and *6*; *white arrowheads* (LAM) and *white lines* (LM) indicate the peaks of the intensity profile shown in supplemental Fig. S4). Upon induction of MSMEG_4247 expression, production of normal sized LAM became even less efficient (compare *black arrowheads* in *lanes 2* and *4*), dwarfed LAM became even smaller (compare *white arrowheads* in *lanes 2* and *4*), and dwarfed LM became greater in intensity and slightly smaller in size (compare *white lines* in *lanes 2* and *4*). These observations suggest less efficient elongation of LM and LAM, being similar to those seen under constitutive overexpression of MSMEG_4247 (see Fig. 3*A*). Thus, MSMEG_4247 can exert its effect on LM/LAM biosynthesis immediately, and the timing appears to be too fast to be explained by secondary mutations.

The Effect of Overexpressed MSMEG_4247 Can Be Alleviated by the Overexpression of MSMEG_4241—Our data suggested that overexpressed MSMEG_4247 dominates the elongating enzymes, preventing the efficient elongation of the linear α1,6-mannose chain. We wanted to test if this effect of MSMEG_4247 overexpression can be competed by the overexpression of an elongating mannosyltransferase, MSMEG_4241. Therefore, we created another mutant in which an episomal vector for acetamide-inducible MSMEG_4241 expression was transfected into the MSMEG_4247 overexpressing strain (used in *lane 3* of Fig. 3). MSMEG_4241 expression was maximized at 4 h after the addition of acetamide (Fig. 5*A*). At this time point, we metabolically labeled cells with [^{3}H]mannose in a pulse-chase experiment. In control cells overexpressing MSMEG_4247 only, dwarfed LM immediately accumulated, and dwarfed

LAM also accumulated over time (Fig. 5*B*). When MSMEG_4241 overexpression was induced, we found little accumulation of dwarfed LM and identified a radiolabeled species migrating at around 35 kDa, which was comparable with wild-type LAM (Fig. 5*B*). The synthesis of normal size LM (~20 kDa) was less prominent, which might be due to the relative overexpression of MSMEG_4241. Next, we examined if the biosynthetic changes induced by the overexpression of MSMEG_4241 can lead into changes in cell wall composition of LM/LAM. Without acetamide induction, dwarfed LM and dwarfed LAM persisted over the 12-h time course (Fig. 5*C*, *left*). Being consistent with the metabolic labeling experiments, a species comparable with wild-type LAM started to appear at around 35 kDa after the 4-h induction and accumulated over the 12-h induction (Fig. 5*C*, *right*). In contrast to metabolic labeling, dwarfed LM persisted during the time course, suggesting a slow turnover rate of this species. We purified dwarfed LAM (from 0-h induction) and LAM-like species (from 12-h induction) by electroelution (Fig. 5*D*) and examined the sugar composition (Fig. 5*E*). The LAM-like species carried a mannan moiety with a size comparable with the wild-type LAM (see Fig. 2*E* for comparison). In contrast, arabinan size was only partially restored, suggesting that the rate of arabinan biosynthesis falls short of that of mannan biosynthesis when both elongating and branching mannosyltransferases are overexpressed in wild-type cells. These data together suggest that the dwarfing effect of overexpressed MSMEG_4247 can be partially overridden by MSMEG_4241 overexpression.

Spatial and Temporal Control of MSMEG_4241 and MSMEG_4247 Expressions in Wild-type Cells—The above results suggested that MSMEG_4247 and MSMEG_4241 function in close collaboration with each other during the synthesis of LM/LAM. Therefore, we predicted that these two enzymes are located

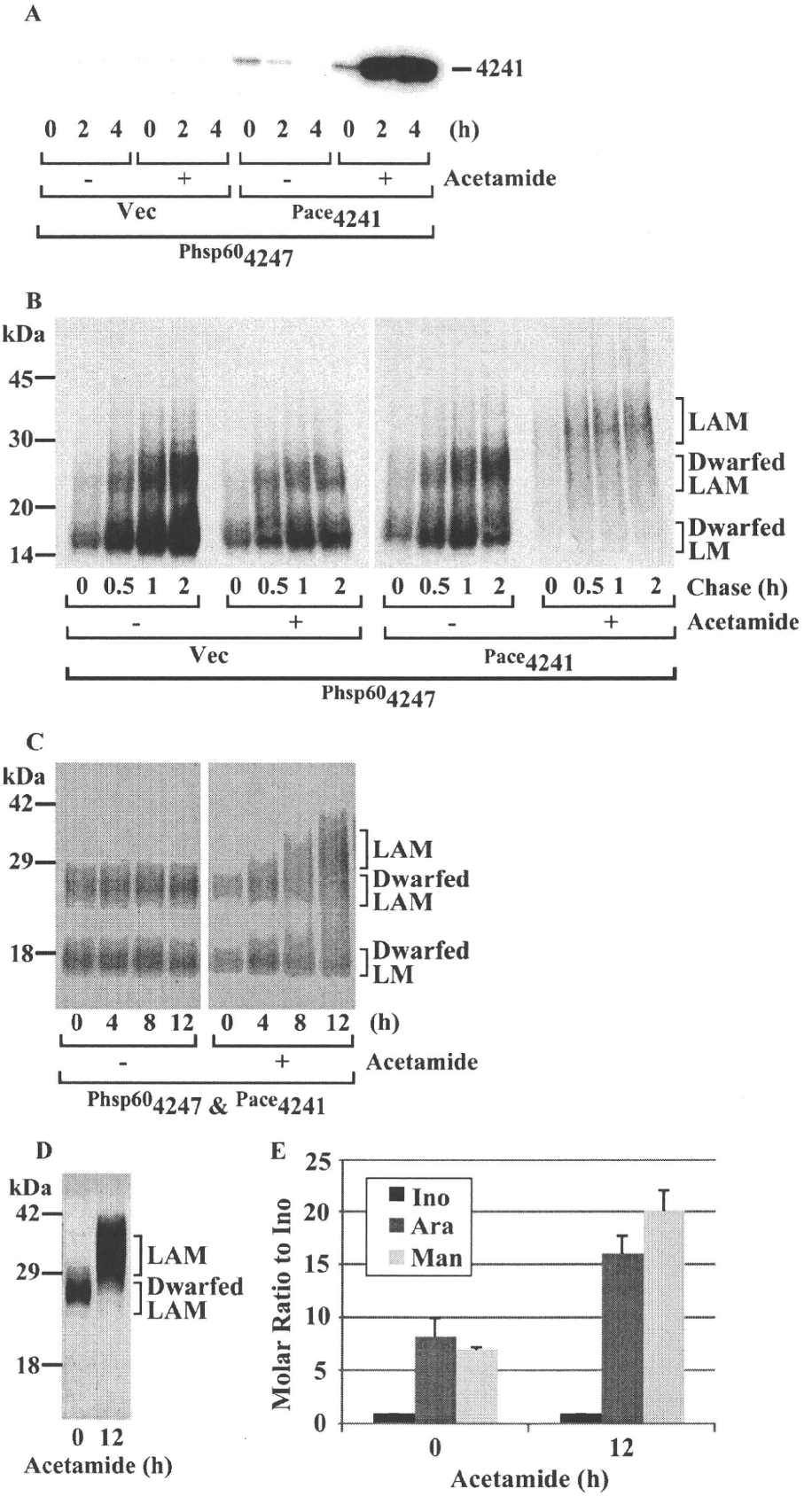

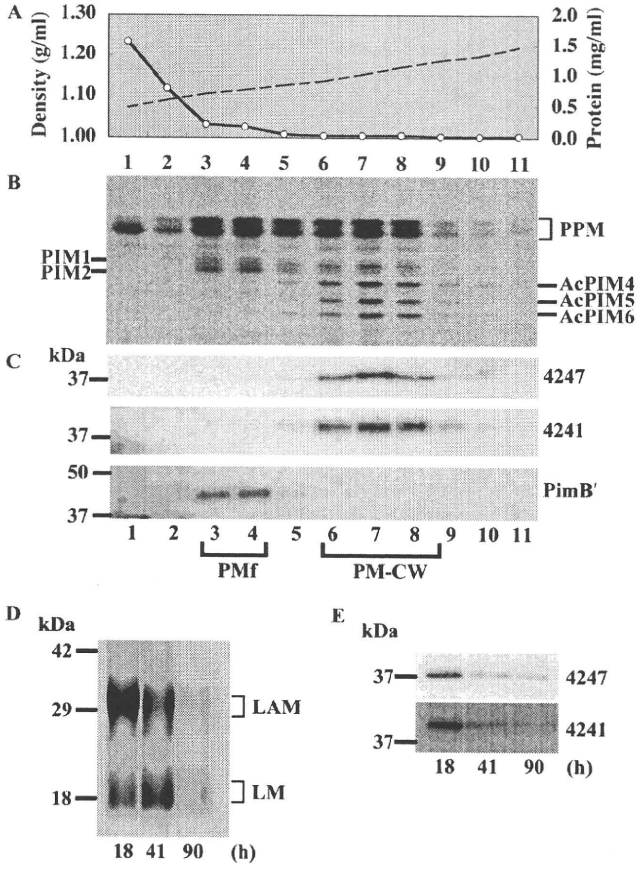

FIGURE 6. **Subcellular localization and growth phase-dependent expression of MSMEG_4247 and MSMEG_4241 in wild-type cells.** *A*, sucrose density (*dashed line*) and protein concentration (*open circle*) profiles of wild-type cell lysate fractionated by a density sedimentation. *B*, PIM biosynthetic activities of each fraction measured by GDP-[^{3}H]mannose radiolabeling. *PPM*, polyprenol-phosphate-mannose. *C*, Western blotting using anti-MSMEG_4247 (*top*), anti-MSMEG_4241 (*middle*), or anti-PimB' (*bottom*) antibodies. *D*, growth phase-dependent changes in LM/LAM levels of wild type cells grown in Middlebrook 7H9 broth. Culture was initiated by 1:100 dilution of a confluent starter culture, and aliquots were collected at the indicated time points, which correspond to logarithmic (18 h), early stationary (41 h), and late stationary (90 h) phases. Purified LM/LAM were separated by SDS-PAGE and visualized by carbohydrate staining. Loading was adjusted for equal cell pellet equivalents. *E*, growth phase-dependent changes in levels of MSMEG_4247 and MSMEG_4241 detected by Western blotting using anti-MSMEG_4247 or anti MSMEG_4241 antibodies. Loading was adjusted to 15 μg of protein/lane.

in the same domain of the plasma membrane. We tested this possibility using subcellular fractions of wild-type *M. smegmatis* (Fig. 6*A*). *M. smegmatis* has two functionally distinct membrane fractions designated PMf and PM-CW (30). PMf fractions contain membrane vesicles free of cell wall components, whereas PM-CW fractions represent plasma membranes tightly associated with the cell wall. PMf and PM-CW membranes can be separated by a sucrose density gradient sedimentation and are responsible for distinct biochemical reactions, such as the early (up to AcPIM2) and late (up to AcPIM6) parts of the PIM biosynthetic pathway, respectively (30) (Fig. 6*B*). As expected from the enriched PIM2 biosynthetic activities in PMf fractions (Fig. 6*B*), PimB' was specifically localized to these fractions (Fig. 6*C*). In contrast, MSMEG_4247 and MSMEG_4241 were both enriched in PM-CW fractions, suggesting that LM/LAM biosynthesis takes place in PM-CW fractions. These data are consistent with MSMEG_4247 and MSMEG_4241 acting in proximity to coordinate the LM/LAM biosynthesis. We have also tested co-immunoprecipitation of these two proteins to show their physical interaction, but it was not successful (data not shown; also see "Discussion"). Another interesting feature of LM/LAM biosynthesis is that it appears to be down-regulated in the late stationary phase (17) (Fig. 6*D*). Because imbalanced expressions of MSMEG_4247 and MSMEG_4241 can result in the production of aberrant forms of LM/LAM, we thought it important for the cells to down-regulate the expression levels of both enzymes in a concerted manner. Indeed, the expression levels of these two proteins were reduced simultaneously in the stationary phase (Fig. 6*E*), in correlation with the reducing levels of LM/LAM. Taken together, MSMEG_4247 and MSMEG_4241 were expressed in a temporally and spatially controlled manner.

Rv2181, an Ortholog of MSMEG_4247, Functions Similarly in M. tuberculosis—To examine whether the phenotypic characteristics of the Δ*MSMEG_4247* mutant were also displayed by other mycobacterial species, we generated an *M. tuberculosis* mutant in which the *Rv2181* gene, the *MSMEG_4247* ortholog, was deleted. The mutant was successfully generated (supplemental Fig. S5, *A* and *B*), and the Δ*Rv2181* mutant showed a smaller sized LAM and disappearance of LM (Fig. 7, *lane 2*), similar to the *M. smegmatis* mutant. When the *Rv2181* gene was introduced with its endogenous promoter region, LM synthesis was restored, and the size of LAM was also restored to that of wild-type LAM (*lanes 3* and *4*). When *Rv2181* was introduced via an integrative vector with Phsp60, the size of LM appeared normal, but the size of LAM appeared slightly smaller (*lanes 5* and *6*). Although the phenotypes are less prominent than those in *M. smegmatis*, these data highlight the conserved role of the α1,2-mannosyltransferase in producing properly sized LM and LAM.

DISCUSSION

Our analysis on MSMEG_4247, a branch-forming α1,2-mannosyltransferase involved in LM/LAM synthesis, revealed unexpected effects of its expression levels on the sizes and

FIGURE 5. **Dwarfing effect of MSMEG_4247 overexpression on LM/LAM can be competed by overexpression of MSMEG_4241.** *A*, acetamide induction of MSMEG_4241 examined by Western blotting using anti-MSMEG_4241 antibody. The MSMEG_4247 overexpression mutant was transfected with either acetamide-inducible MSMEG_4241 expression vector (*^{Pace}4241*) (transfected with pYAB262) or empty vector (*Vec*) (transfected with pJAM2) and incubated with (+) and without (−) acetamide for the indicated period to induce MSMEG_4241 expression. The loading was adjusted to 5 μg of protein/*lane*. *B*, metabolic labeling with [^{3}H]mannose. Cells were preincubated with (+) or without (−) acetamide for 4 h, pulsed for 15 min with [^{3}H]mannose, and then chased in the presence of excess non-radioactive mannose for up to 2 h. *C*, changes in total LM/LAM profiles after induction of MSMEG_4241 expression in MSMEG_4247 overexpression mutant. LM/LAM were separated by SDS-PAGE and visualized by carbohydrate staining. *D*, dwarfed LAM at 0 h and LAM-like species at 12 h after acetamide induction, shown in *C*, were purified by electroelution, and the purities were confirmed by SDS-PAGE and carbohydrate staining. *E*, compositional analysis of LAM-like species produced after MSMEG_4241 overexpression. Trifluoroacetic acid-hydrolyzed carbohydrates were quantified by HPAEC. Data are presented as molar ratio relative to inositol. Averages of triplicate measurements with S.D. values are shown.